Geol. Mag.: page 1 of 19 © Cambridge University Press 2017
doi:10.1017/S0016756817000498

Upper Jurassic travertine at El Macanudo, Argentine Patagonia: a fossil geothermal field modified by hydrothermal silicification and acid overprinting

DIEGO M. GUIDO*† & KATHLEEN A. CAMPBELL‡

*CONICET and Facultad de Ciencias Naturales y Museo, Universidad Nacional de La Plata, Instituto de Recursos Minerales (INREMI), Calle 64 y 120, La Plata (1900), Argentina
‡School of Environment, University of Auckland, Private Bag 92019, Auckland 1142, New Zealand

(*Received* 24 May 2016; *accepted* 18 May 2017)

Abstract – The Deseado Massif hosts numerous Late Jurassic (150 Ma) fossil geothermal systems related to an extensive volcanic event developed in a diffuse extensional back-arc setting. Detailed mapping, petrography and mineralogical observations of El Macanudo outcrops verify that it represents a hot-spring-related travertine partially replaced by silica and delineated by six sedimentary facies. These are large concentric cones (F1), laminated vertical columnar structures (F2), porous layers (F3), shrubby and irregular lamination (F4), low-amplitude wavy bedding (F5) and mounds and breccias (F6). The Macanudo Norte Outcrop rocks constitute a silica-replaced travertine sequence, with development of large conical stromatolites in a deep pool or geothermally influenced shallow lacustrine environment, surrounded by a subaerial travertine apron terrace; whereas, the Macanudo Sur Outcrop is a subaerial travertine mound sequence. Structurally controlled vent areas occur in both northern (F1) and southern (F6) outcrops, mainly located along regional NNE- and ENE-trending faults. The other sedimentary units display a concentric distribution of travertine facies with respect to the interpreted vent areas. The El Macanudo palaeo-hot spring deposit is situated in an eroded Jurassic volcanic centre, and records a complex evolutionary-fluid history. The sediments archived three different Jurassic events, when large and long-lasting hydrothermal systems were active across the region. This relative temporal sequence was formed by: (1) travertine precipitation; (2) development of a silica cap, where early silicification was responsible for exceptional preservation of some stromatolitic fabrics; and (3) acid alteration, recorded by dissolution textures and clay formation, and caused by a palaeo-phreatic water-level drop.

Keywords: hot spring, Jurassic, Argentina, travertine, palaeoenvironment, silicification, hydrothermal alteration

1. Introduction

The El Macanudo hot spring deposit (Schalamuk *et al.* 1997, 1999) is located in the Deseado Massif geological unit, Santa Cruz province, southern Patagonia, Argentina. This region is a 60,000 km^2 area characterized by an extensive (> 30,000 km^2), Middle to Late Jurassic, bimodal volcanic event known as the Bahía Laura Complex (BLC), including Chon Aike rhyolites intercalated with Bajo Pobre andesites, and reworked volcaniclastic rocks of the La Matilde Formation (Fig. 1; Echeveste *et al.* 2001; Guido, 2004; Guido *et al.* 2006). In broad terms, La Matilde strata, including fossil hot spring deposits, are found at the top of the sequence together with intermediate to silicic lava domes of the BLC, and accumulated in a mature (quiescent) phase of volcanism during Late Jurassic time (Guido, 2004). Collectively, these rocks are part of the Chon Aike Silicic Large Igneous Province (SLIP), which extends from Argentine Patagonia to Antarctica (Pankhurst *et al.* 1998), and which developed in a diffuse extensional back-arc setting associated with the opening of the South Atlantic Ocean (cf. Richardson & Underhill, 2002).

Over a ~30 Ma interval in Middle to Late Jurassic time (*c.* 178–151 Ma), extension, magmatism and a high thermal gradient produced BLC volcanism and related hydrothermal mineralization in the Deseado Massif, including economic gold- and silver-bearing, mainly low-sulphidation-type epithermal quartz veins, and numerous hot spring occurrences (Fig. 1). The local and regional geological context of the numerous geothermal and significant epithermal deposits of the Deseado Massif, and their alignment along major lineaments as confirmed by aeromagnetic data, together indicate structural control of Jurassic hydrothermal activity, with the focus of dynamic fluid up-flow (cf. Renaut & Jones, 2011*a*) along the western and northern horst-like boundaries of the Massif itself (Guido & Schalamuk, 2003; Guido & Campbell, 2011).

Deseado Massif hot-spring-related deposits comprise mostly travertines, some siliceous sinters and plant-rich cherts, and are hosted in tuffs and reworked volcaniclastic sediments within fluvio-lacustrine

†Author for correspondence: diegoguido@yahoo.com

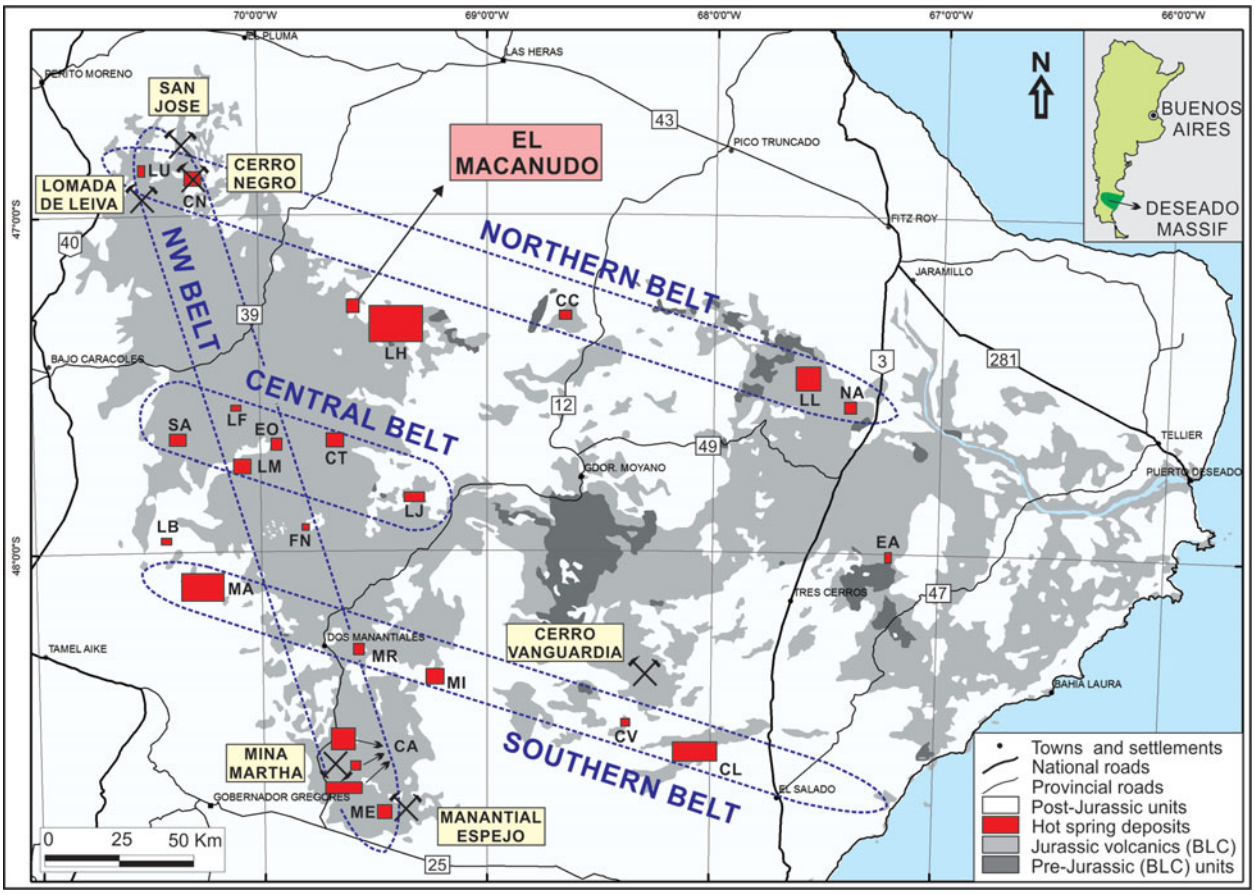

Figure 1. (Colour online) Simplified geological map of the Deseado Massif showing all 23 known hot spring localities (red boxes, with El Macanudo study area labelled) aligned in four major structural belts, and regional gold–silver epithermal mines (modified from Guido & Campbell, 2011). Inset shows the position of the Massif in Argentina. Abbreviations: LU – La Unión; CN – Cerro Negro; CC – Cerro Contreras; LL – La Leona; NA – Cañadón Nahuel; LH – La Herradura; EA – El Águila; SA – San Agustín; LF – La Flora; LM – La Marcelina; EO – Esperanza Oeste; CT – Cerro Tornillo; LJ – La Josefina; FN – Flecha Negra; LB – La Bajada; MA – La Marciana; MR – La María; MI – Monte Illiria; CV – Cerro Vanguardia; CL – Claudia; CA – Cerro 1 Abril; ME – Manantial Espejo.

settings over a 230 × 230 km area (Fig. 1; Guido & Campbell, 2011). A regional hydrothermal silicification event overprinted many of these interbedded hot spring and volcaniclastic rocks during Late Jurassic time (Guido *et al.* 2002), indurating the deposits and thus generally increasing their long-term preservation potential. Nonetheless, depending on the extent of the silicification and local post-depositional history (i.e. diagenetic recrystallization, subsequent hydrothermal alteration), original textural and compositional details became obscured at a number of sites. For some deposits that underwent pervasive early silicification, hot-spring-related facies of exceptional preservation also can be found, such as the San Agustín sinter (SA of Fig. 1; Guido *et al.* 2010; Channing *et al.* 2011; García Massini *et al.* 2012), the Cerro Negro travertine (CN of Fig. 1; Guido & Campbell, 2012) and the Claudia sinter and travertine (CL of Fig. 1; Guido & Campbell 2014).

The Jurassic Patagonian rocks subsequently were buried by Cretaceous and Cenozoic continental and marine passive margin successions (Giacosa *et al.* 2010), and then unearthed with minimal structural disturbance to expose intact, erosional windows into 23 mapped subaerial and/or sub-lacustrine geothermal systems (Guido & Campbell, 2011). At several locations, the fossil palaeo-surface expressions of hydrothermal activity are recorded, with diverse geothermal landscapes represented. Such three-dimensional spatial associations of these fossil geothermal facies assemblages enable detailed palaeogeographic, palaeoenvironmental and palaeohydrologic reconstructions (e.g. Guido & Campbell, 2009, 2012, 2014; Guido *et al.* 2010; Campbell *et al.* 2015*a*). They also provide glimpses into the inner workings of entire volcanic–epithermal–geothermal systems rarely possible in other older or younger continental hydrothermal settings elsewhere in the world.

The aim of this study is to evaluate in detail the geological context and diverse facies associations of the hot-spring-related deposits at El Macanudo, which are exposed over a 1 km^2 area and may be divided into northern and southern portions. The northern part (here designated Macanudo Norte) was one of the first supposed sinter occurrences noted in the Deseado Massif (Schalamuk *et al.* 1997). It later was

reinterpreted as a travertine deposit mostly replaced by silica (Schalamuk *et al.* 1999), which is a type of pseudosinter (cf. Guido & Campbell, 2012), in its higher topographic levels. Neither the northern nor southern (Macanudo Sur) areas of this palaeogeothermal field have been described in detail. This Upper Jurassic hot spring deposit exhibits surface geothermal manifestations comparable to Pleistocene–Recent, geothermally affiliated deposits of Yellowstone National Park (Wyoming, USA), the Kenyan Rift Valley and elsewhere. Overall, the El Macanudo fossil geothermal system yields textural details of variable quality, owing to both the differential preservation potential of particular subaerial versus subaqueous facies, as well as to the timing and extent of carbonate diagenesis, silica replacement and the newly identified, late-stage hydrothermal (acid) alteration in some areas. Hence, El Macanudo provides an opportunity to assess the impact of depositional and post-depositional history on hot spring (micro)facies and microbial fossil preservation in hot spring travertines, thereby yielding clues to the processes affecting the development and long-term preservation potential of Lagerstätte ('mother lode' deposits of exceptional fossil preservation) in epithermal settings and, more broadly, in extreme environments of the geological record.

2. Thermal spring fluids and facies

Continental hot spring deposits of high-enthalpy hydrothermal systems develop as chemical precipitates derived from thermal waters discharging at the Earth's surface, typically in the temperature range of ~35–100 °C, and located in fluvio-lacustrine settings of active tectonic and volcanic terrains near plate boundaries (Renaut & Jones, 2000, 2011*a*). The fluids originate as mainly meteoric waters, in places supplanted with minor connate, magmatic or metamorphic components, which convectively circulate above magmatic intrusions, and by conductive heat transfer through the shallow crust, via faults, fractures and permeable horizons (Henley & Ellis, 1983; Renaut & Jones, 2011*a*). Heated fluids rise and may boil at subterranean levels with decreasing pressure towards the surface, causing steam separation that results in surface discharges of hot springs and geysers (liquid-dominated) or fumaroles and steaming ground (steam-dominated) (Henley & Ellis, 1983; Renaut & Jones, 2011*a*). The mineralogy of the precipitates accumulating in association with the surface hot spring manifestations, as well as the biota that inhabit areas of thermal discharge, are fundamentally controlled by water composition (Jones & Renaut, 2011). Hence, geothermal fluids are generally classified into chloride, sulphate and bicarbonate waters by dominant anion (Henley & Ellis, 1983; Nicholson, 1993; Renaut & Jones, 2011*a*), although mixed anionic composition types are also known (e.g. acid–sulphate–chloride; Ellis & Wilson, 1961). Alkali chloride geothermal fields are derived from chemical interactions of hot water with volcanogenic host rocks to a few kilometres crustal depth, creating solute-rich, saline geothermal reservoirs (up to 400 °C), with magmatically driven fluid circulation enabling migration to the surface of these deep, chloride-rich fluids, where they are expelled as clear, near-neutral pH hot springs and geysers over-saturated in silica and which, upon cooling and evaporation, precipitate relatively thick (decimetres to tens of metres) siliceous sinter (Fournier & Rowe, 1966; Fournier, 1985; Renaut & Jones, 2011*a*,*b*). The rising thermal fluids may move laterally through permeable, near-surface units and mix with shallow groundwater, particularly around the margins of up-flow zones, to produce acid–sulphate springs as common geothermal manifestations (Henley & Ellis, 1983; Renaut & Jones, 2011*a*). In particular, oxidation of H_2S and other gases in steam-heated, oxygenated groundwater may exit to the surface in the vapour phase as acidic fumaroles and steaming ground, or condense in perched water tables to form acid–sulphate springs and acid lakes that are often associated with deposits of silica residue, native sulphur and hydrothermal alteration minerals (e.g. kaolinite, jarosite, alunite) (e.g. Rodgers *et al.* 2004; Renaut & Jones, 2011*a*). In some locations, mixing of acid–sulphate and chloride waters will deposit thin siliceous sinters (a few centimetres thick) with distinctive textures and biotas (Schinteie, Campbell & Browne, 2007). Furthermore, concentration of dissolved CO_2 in groundwater around the peripheries of geothermal fields and at sites distant from volcanic activity may generate neutral to alkaline bicarbonate springs of variable temperature, and form subaerial travertine mounds and terraces of variable thickness (a few centimetres to tens of metres) via loss of CO_2 from the discharging fluids at atmospheric pressure (Pentecost, 2005; Renaut & Jones, 2011*a*). Subaqueous (lacustrine) hot springs also form travertine with distinctive cone geometries (e.g. Guido & Campbell, 2012). In areas of low topographic relief and limited potential for lateral flow of fluids near the land surface, both acid and alkaline springs may form in close proximity (e.g. Renaut & Jones, 2011*a*; Jones & Renaut, 2012). Overall, the thickness and extent of the sinter or travertine deposits developed in geothermal areas are mainly controlled by volume and duration of fluid flow as well as by the degree of over-saturation of fluids in silica and bicarbonate species with respect to ambient temperature (Henley & Ellis, 1983; Guido & Campbell, 2014). These are, in turn, influenced by tectonics (e.g. faults as baffles and/or barriers to fluid flow, reactivation), volcanism (e.g. water table elevation, heat source), host rock geology (e.g. dissolved mineral concentration, permeability) and climate (e.g. fluid volume, water table fluctuations) (e.g. Sibson, 1987; Sturchio, Dunkley & Smith, 1993; Rowland & Simmons, 2012; Guido & Campbell, 2014; Sillitoe, 2015).

Calcareous terrestrial hot spring deposits, or thermogene travertines, are porous, laminated carbonates

that precipitate from mineral-laden thermal waters, with both abiogenic and biogenic influences on their deposition (Pentecost, 1990, 2005; Koban & Schweigert, 1993; Guo & Riding, 1994). Thermogene travertines are distinguished from the more common meteogene travertines by the origin of their dissolved CO_2, which is derived from deep, high-enthalpy fluid reservoirs in the former setting, and from the soil and atmosphere in the latter (Pentecost, 1993; Gibert *et al.* 2009). Thus, as used here, thermogene refers to the fluid source rather than necessarily the surface temperature of the spring, which for travertines can vary widely (Pentecost, 2005). For example, across the western USA, travertine-depositing springs range from 5 to 95 °C, with most between 10 and 30 °C (Chafetz & Folk, 1984). In essence, thermogene travertines are produced by inorganic $CaCO_3$ precipitation owing to degassing and evaporation of the debouching thermal spring waters, although microbial surface catalysis (templating) may also stimulate carbonate precipitation (Pentecost, 1990; Guo & Riding, 1994; Chafetz & Guidry, 1999). In contrast, tufa tower, cone and mound-like deposits (a type of meteogene travertine) generally differ from hot spring travertines by a lack of terraces, a predominance of moulds of higher aquatic plants, formation under relatively cooler (e.g. groundwater seepage) conditions in normal freshwater environments and their often greater geographic extent (e.g. within and around margins of shallow lakes) (e.g. Koban & Schweigert, 1993; Rosen, Arehart & Lico, 2004; Pentecost, 2005). In practice, however, it is difficult to apply current classifications of tufa versus travertine to (sub)fossil systems where water is no longer flowing, and the distinction between these two terms has been blurred owing to inconsistent usage (Pentecost, 2005; Jones & Renaut, 2010).

Cooling and evaporation of discharging thermal fluids around subaerial hot spring vent and mound sites cause precipitation of hydrous, non-crystalline opal-A in the case of alkali chloride sinter formation (White, 1967; Jones & Renaut, 2003*a*,*b*; Jones, Renaut & Owen, 2011) and aragonite and calcite precipitation in the case of thermogene travertine deposition (Pentecost, 1990, 2005; Fouke *et al.* 2000). This often rapid mineralization may coat and entomb the available biotic and abiotic surfaces; thus, the preservation potential of physical, chemical and biological signatures in sinters and travertines make them valuable archives of the environmental, geothermal and geological processes operating during periods of hot spring activity (e.g. Sturchio, Dunkley & Smith, 1993; Cady & Farmer, 1996; Farmer, 2000; Fouke *et al.* 2000; Lynne *et al.* 2005, 2008; Handley & Campbell, 2011; Lynne, 2012; Campbell *et al.* 2015*a* ,*b*).

Sinter and travertine facies models (Guido & Campbell, 2011, their fig. 3, p. 40) correlate distinct macro- and microscopic mineral textures to positions upon the cooling discharge apron (~100 °C to ambient) (Cady & Farmer, 1996; Farmer, 2000; Fouke *et al.* 2000; Campbell *et al.* 2001; Guido & Campbell, 2011; Lynne, 2012). Subaerial sinter and travertine facies assemblages may be broadly grouped into three main categories: (1) vent mound or spring-vent pool and proximal slope (> 65 °C), (2) mid-apron terraces (< 65–45 °C) and (3) distal apron to marsh (< 45 °C) (Guido & Campbell, 2011). Biotic community composition and distributions follow temperature and fluid chemistry gradients down the discharge apron, which show broad similarities between alkali chloride and bicarbonate springs, but also exhibit some distinct differences, manifesting in somewhat variable sedimentary textures between the two spring types (e.g. Guido & Campbell, 2011, their table 1, p. 40). With respect to post-depositional modification of ancient hot spring deposits, siliceous sinters naturally undergo a series of silica mineral phase transformations as structural water is lost during diagenesis (i.e. change from non-crystalline opal-A to microcrystalline quartz over time; Herdianita *et al.* 2000; Lynne & Campbell, 2003; Lynne *et al.* 2006, 2007). Moreover, travertine carbonate is quite sensitive to recrystallization such that diagenesis may be rapid and readily destroy environmentally indicative fabrics (e.g. Renaut, Morley & Jones, 2002; Jones & Renaut, 2010; Guido & Campbell, 2011, 2012). Early diagenetic silicification, common in volcanic terrains and occurring in both sinter- and travertine-forming settings, may facilitate cases of exceptional preservation of biotic and abiotic fabrics of (palaeo)environmental significance (e.g. Trewin, Fayers & Kelman, 2003; Guido *et al.* 2010; Guido & Campbell, 2012).

3. Materials and methods

Field mapping aided by satellite imagery was conducted in Santa Cruz province, Patagonia, Argentina, in August 2012, and rock samples were cut and photographed in the School of Environment at the University of Auckland. Twenty-nine representative thin-sections (2 × 4 cm dimensions, 30 μm thick) were made from about 50 rock samples and viewed under plane and polarized light microscopy. Energy dispersive X-ray spectroscopy (EDS/EDAX) was undertaken at the Research Centre for Surface and Materials Science, University of Auckland, with a Si–Li (lithium-drifted) EDS detector on a FEI Quanta 200 F operating at 25 kV to obtain semi-quantitative compositional data for selected surfaces.

4. Results

4.a. Geology of the El Macanudo area

The geology of the El Macanudo area (Fig. 2) is represented by Jurassic volcanic rocks of the Bahía Laura Complex (BLC, Feruglio, 1949; Guido, 2004) that are partially covered by Eocene basaltic flows and Holocene alluvial–colluvial deposits. The El Macanudo hot spring deposit is situated at the southeastern edge of a 7 × 3 km, NW-elongated low area where Mirasol Lake

Table 1. Palaeoenvironmental and palaeohydrologic interpretation of the six described thermogene travertine facies (F1–F6) at El Macanudo, Deseado Massif, Patagonia, Argentina

Facies	Subfacies	Facies interpretation	Hydrologic interpretation	Silica overprint	Acid overprint	Inferred temp.
Concentric Cones (F1)		Geothermal vent conduits	Subaqueous exit point of fluid conduits	Yes	Yes	High
Vertical Columnar Structures (F2)		Mid-temperature pool floor	Relatively deep pool level	Yes	Yes	Moderate
Porous Layers (F3)			Relatively shallow pool level			
Lamination (F4)	Irregular lamination (F4.1)	Travertine terraces	Laminar fluid flow	Yes	Yes	Moderate to low
	Shrubby lamination (F4.2)			Patchy	Partial	
Low-amplitude wavy bedding (F5)		Base of travertine mound	Laminar fluid flow	Patchy	No	Moderate to low
Mound and breccia features (F6)		Conduits	Subaerial	No	No	High

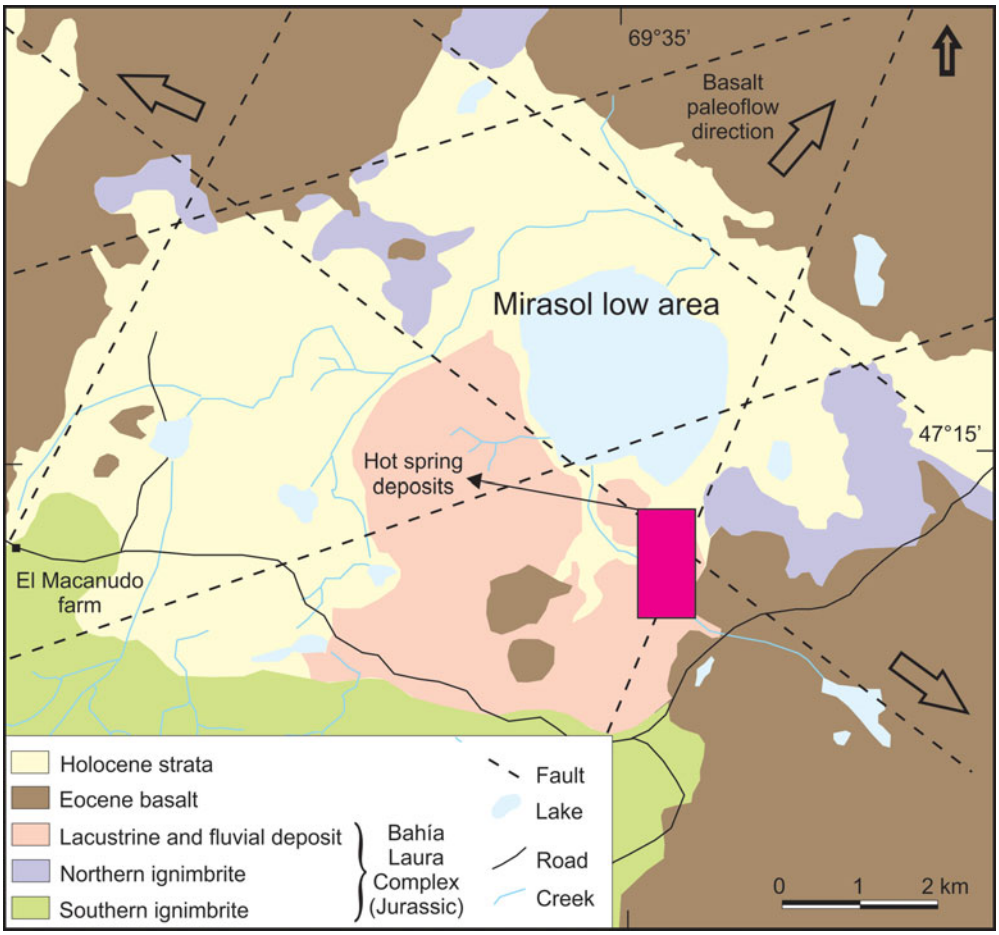

Figure 2. (Colour online) Geological map of the El Macanudo – El Mirasol area (modified from Schalamuk *et al.* 1999). Magenta rectangle indicates the hot spring area, shown in more detail in Figure 3. Basalt palaeoflow direction indicators suggest the present-day Mirasol low area was an early Cenozoic topographic high, a possible (now eroded) volcanic centre (discussed further in the text).

is located (designated Mirasol low area in Fig. 2). It is delineated by NW- and NNE-trending faults, creating a four-sided geometric area, and is covered by Eocene flood basalts on three of the four sides. There also are ENE-trending lineaments in the study area (Fig. 2).

The Late Jurassic volcanic rocks include two types of ignimbrites as well as volcanic reworked materials (Schalamuk *et al.* 1999). Volcanic reworked deposits occupy a ~4 km^2 area and comprise ash fall tuffs intercalated with lacustrine and fluvial deposits assigned to the La Matilde Formation. The El Macanudo hot

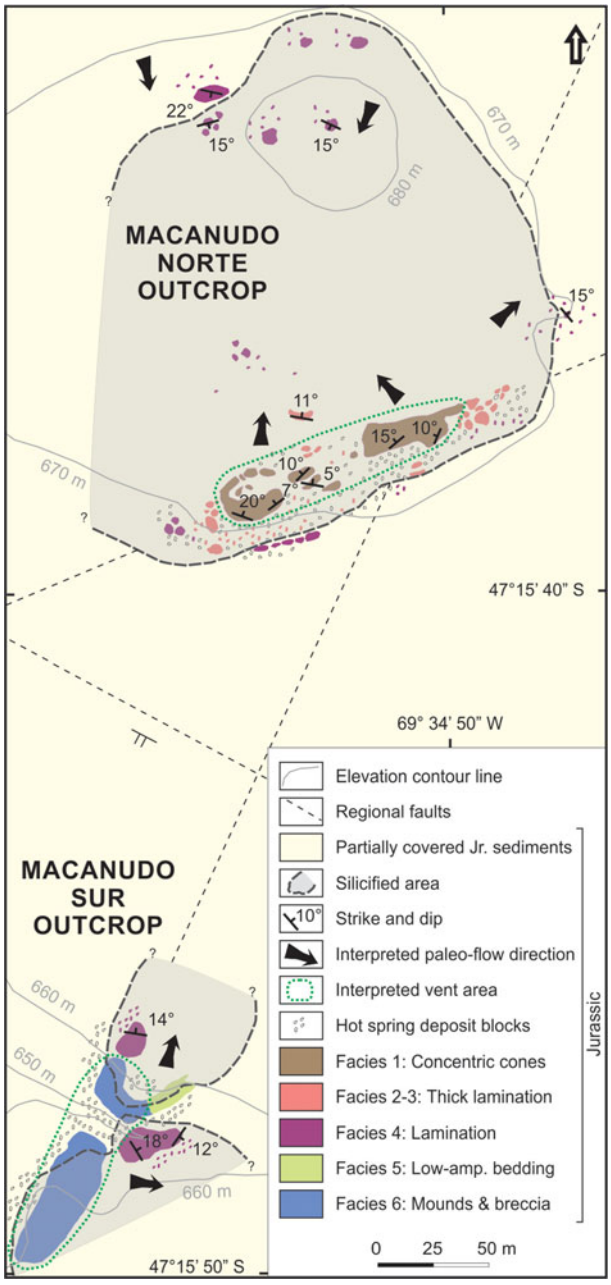

Figure 3. (Colour online) Detailed geological and facies map for the El Macanudo hot springs area, which includes six hot-spring-related sedimentary facies (F1–F6) variably preserved as travertine or silicified travertine (pseudosinter). The Macanudo Norte Outcrop is exposed at approximately the 670 m elevation contour; whereas, the Macanudo Sur Outcrop is at approximately 660–650 m elevation.

spring deposits are interbedded with this unit along its eastern outcrop area, which is spatially related to a major NE-trending fault that constrains the Mirasol low area to the east (Fig. 2). The hot springs are associated with laterally pervasive, silicified tuffaceous and lacustrine strata, and intense argillic alteration in the unsilicified tuffs and volcaniclastic rocks.

Two outcrops expose the hot spring deposits, separated by a NW-trending normal fault (Fig. 3). The Macanudo Norte Outcrop, previously described as the Macanudo Hill outcrop (Schalamuk *et al.* 1997, 1999), constitutes silicified travertine hot spring facies above 670 m altitude (Fig. 4a). The Macanudo Sur Outcrop is composed of carbonate and siliceous hot spring deposits that occur at a lower altitude (650–660 m). These two hot spring outcrops were mapped and studied in detail to define six sedimentary facies related to surface geothermal activity (Table 1). The Macanudo Norte Outcrop contains four spring-related facies. Specifically, large concentrically layered cones up to 1 m high (F1 of Fig. 4b) are underlain by irregularly alternating, thickly laminated horizons (centimetres to a few decimetres thick) of vertical columnar structures (F2) and porous layers (F3) (Fig. 4b). The F1–F3 facies are surrounded by a laminated facies (F4) that is tabular in outcrop (Fig. 4c). The Macanudo Sur area exhibits the same laminated facies (F4) found at Macanudo Norte, along with two additional facies: low-amplitude wavy bedding (F5) overlain by mounds and breccias (F6) (Fig. 4d, e). A detailed description of these six hot-spring-related facies follows.

4.b. El Macanudo hot spring facies

4.b.1. Facies 1 (F1): concentric cones

This siliceous facies is exclusively located at the Macanudo Norte Outcrop (Fig. 3). It is positioned at the highest part of the outcrop, along the southern border, and occurs as a 125 × 30 m ridge aligned with a regional ENE-trending fault. This is the most morphologically distinctive facies at El Macanudo, and therefore attracted the attention of Schalamuk *et al.* (1997, 1999) in an initial survey of the area. The concentrically laminated cones are composed of individual or groups of pipe-shaped to conical, stromatolitic vertical structures, preserved in their original environmental position (Figs 4b, 5a–c). They are composed of thin (< 1 cm), wavy to crenulated, concentric bands arranged in cylindrical to ovoidal forms in transverse section (Fig. 5b). Individual concentric cones range in diameter from centimetres to < 1 m, and in height up to 1 m, and commonly occur in groups as mounded features (Fig. 5a). The concentric cones display strong porosity in hand sample (Fig. 5c), preserved normally as elongated holes mainly parallel to the stromatolitic lamination, with their upward terminations (where unbroken) exhibiting cone-shaped tips (Fig. 5a, inset). In thin-section, irregularly rounded pores to elongate holes are clearly evident, with some cross-cutting laminae but most others extending parallel to the lamination (Fig. 5d). The pores are oriented along and between the thin stromatolitic walls, and display concave internal borders, many of which are coated by a thin reddish layer (Fig. 5d). The matrix is silicified and recrystallized from the original carbonate, and chalcedonic spheres and quartz crystals are observed under the microscope. In only a few places is the original carbonate texture preserved, where it encloses remnants of poorly preserved organic matter and/or microbes (Fig. 5e).

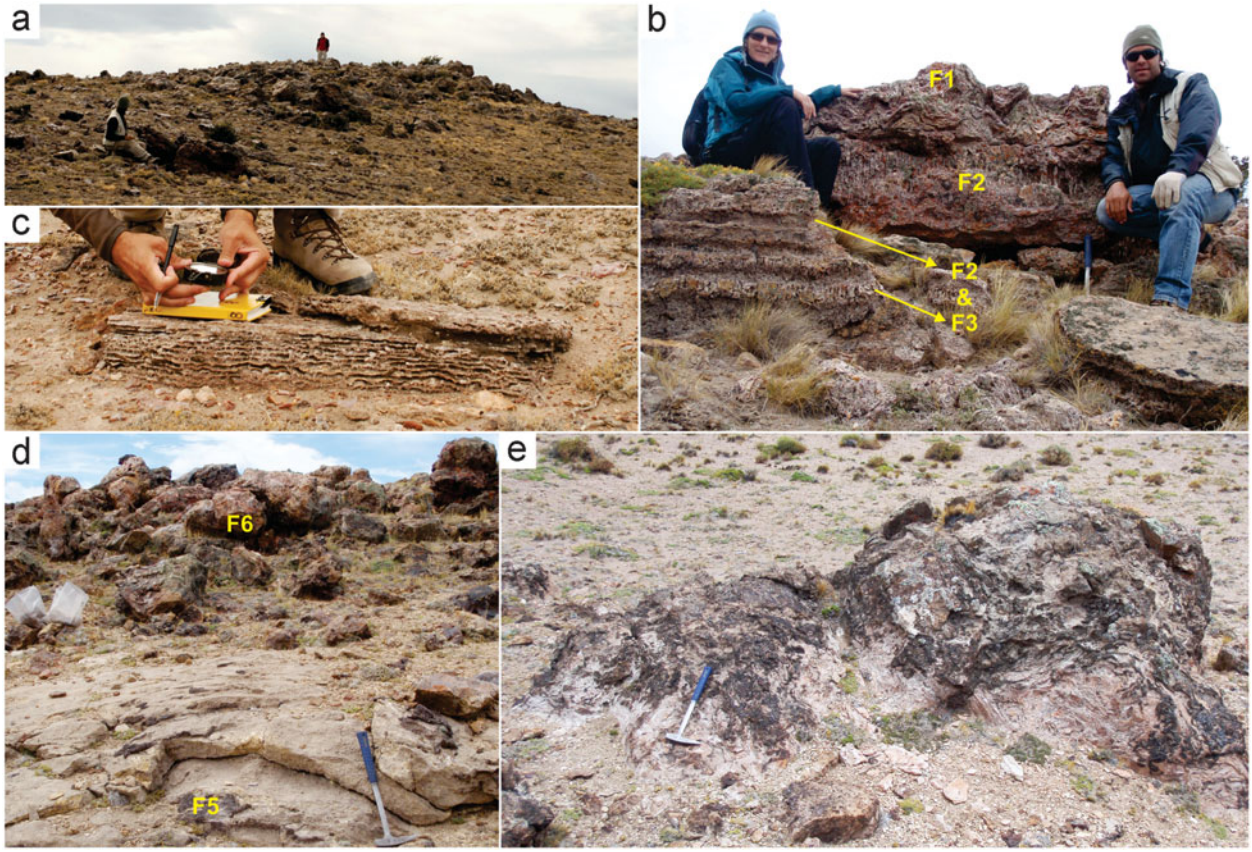

Figure 4. (Colour online) Photographic overview of the El Macanudo hot spring area and its six different facies types, F1–F6. (a) Macanudo Norte Outcrop; view to the top of the 670 m contour hill. (b) F1 to F3 horizons cropping out at Macanudo Norte: concentric cones (F1), and vertical columnar structures (centimetre- to decimetre-scale) (F2) alternating with porous structures (F3). Note the different heights of the vertical columnar horizons (F2), which are likely related to palaeo-hot spring water depth. (c) Subcrop of the laminated facies (F4) at Macanudo Norte. (d) Macanudo Sur outcrops of low-amplitude wavy bedding (F5), in close spatial association with silicified mounds (F6). (e) Macanudo Sur Outcrop of travertine mound (F6) comprising irregularly and concentrically layered stromatolitic features. Hammer for scale is 40 cm long.

4.b.2. Alternations of Facies 2 (F2): vertical columnar structures; and Facies 3 (F3): porous layers

These two facies commonly occur together as horizontal intercalations of silica-rich layers (thick laminae to thinly bedded) underneath and/or distributed around the concentric cones (F1) facies (Figs 4b, 6a, b). The F2 facies is characterized by thickly laminated, siliceous columns of different heights (1–25 cm) and variable quality of preservation. These vertical elements are, in places, thin and wrinkly to wavy (Fig. 6a, b), columnar (Fig. 6c) or botryoidal (Fig. 6d), and form circular features as observed in plan view.

The microtextures of these vertical columnar F2 structures have oriented rounded holes (Fig 6e), with a recrystallized matrix that contains some chalcedony spheres, preserved patches of the original microbial fabrics and scattered plant fragments. Two generations of holes can be distinguished (Fig. 6e). Elongated to lenticular, fingernail-shaped holes are common, which are yellowish to reddish in colour in their concave internal portions (labelled b in Fig. 6e; Fig. 6f). In places, the walls are broken (Fig. 6f) and the once hollow interiors completely or partially filled by quartz crystals. In addition, circular to irregular holes are present, with an internal, thin, reddish coating (labelled v in Fig. 6e, g). The F3 facies is mainly composed of very porous massive to stratified silica layer(s) (Fig. 6h). Irregular holes are homogenously distributed (i.e. not oriented) and internally show the same reddish coating (Fig. 6i). The matrix mainly consists of quartz crystals with a mosaic texture, with some patchy remnants of the original microbial fabric, plant debris and a few chalcedony spheres.

4.b.3. Facies 4 (F4): lamination

A large area of layered silicified carbonate with ~1 cm thick laminae constitutes this facies. The lamination is distributed around the F1 to F3 outcrop area (Fig. 3) at the Macanudo Norte Outcrop. This facies is also found in the higher parts of the Macanudo Sur Outcrop. Several morphological varieties are included in this facies, which show a gradation in alteration and diagenesis. Most of them superficially appear to be siliceous sinter; hence, the term 'pseudosinter' (cf. Guido & Campbell, 2011) can be applied to this lithofacies (Figs 4c, 7a). Two main end-members were defined:

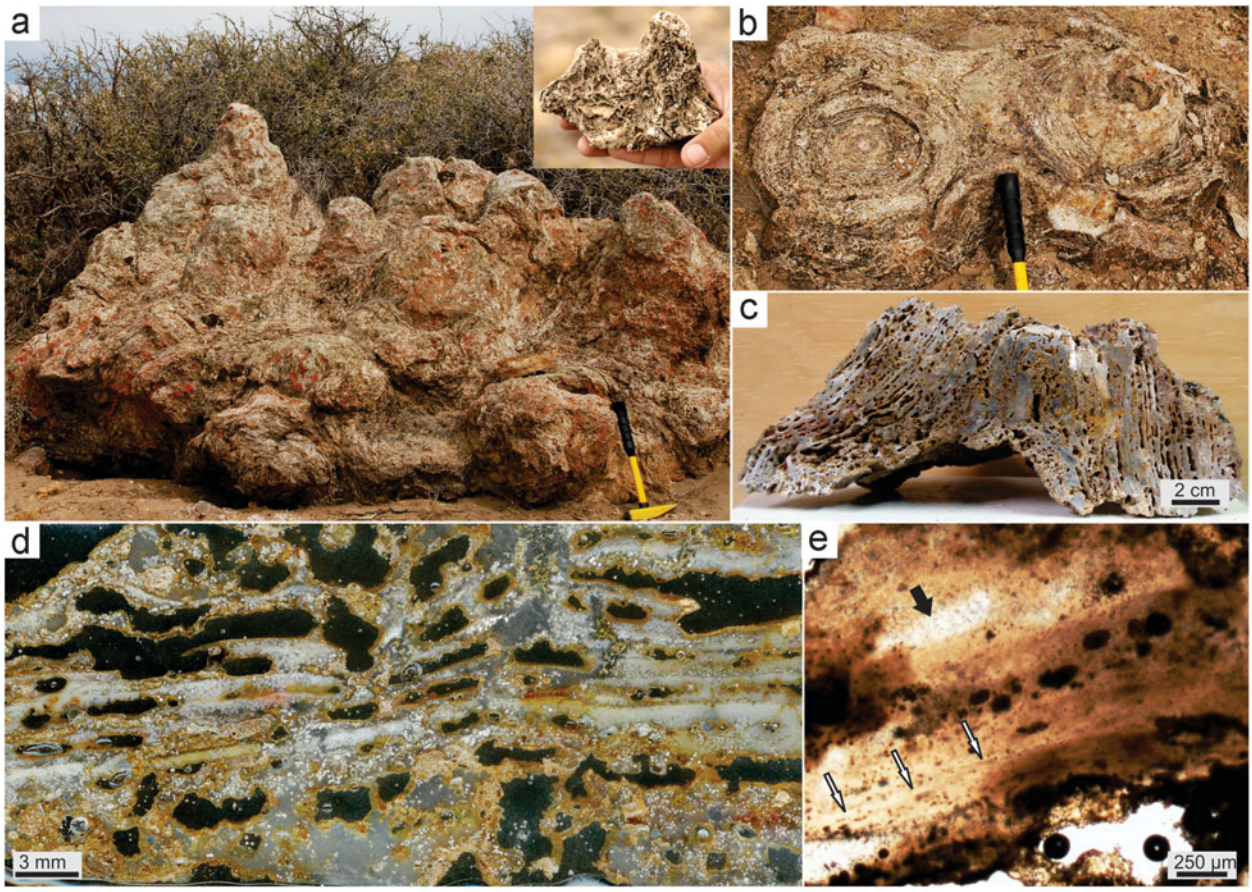

Figure 5. (Colour online) Photographs and photomicrographs of the concentric cone facies (F1) at the Macanudo Norte Outcrop. (a) Vertical views of a group of coalescent concentric cones, and a detail of an upper cone termination (inset). (b) Detail of two eroded, laterally linked concentric cones in plan view, with preserved stromatolitic fabric. (c) Cut slab of a concentric cone (vertical section view) showing typical high porosity of the rock, patchy silicification (grey) and oxidation (red Fe-staining). (d) Thin-section of a concentric cone in transverse section, showing pervasive, randomly oriented but dense, irregular pores (black, open spaces) and oxidation (red tint) following stromatolitic lamination (white, quartzose, slightly undulatory horizons). (e) Detail of a patchy remnant of silicified travertine in thin-section, with possible preserved microbial fabric including faint wavy laminae (thin arrows), and possible amygdaloidal bubble, now filled with clear quartz, from inferred photosynthetic degassing of a microbial mat (thick arrow). The surrounding area of the thin-section (not shown) is very poorly preserved, with no discernible primary fabric. Hammer for scale is 35 cm long.

an irregular lamination type (F4.1) occurring adjacent to the F1 to F3 facies distribution area, and a shrubby lamination type (F4.2) found in a geographically more extensive area, especially to the north, and which exhibits excellent preservation at one location (Fig. 4c).

F4.1: irregular lamination. These deposits have irregular, white to yellowish and brownish to black, intercalated laminae (Fig. 7b). Under the microscope, the colours of the dark and light laminae are reversed. Specifically the brownish to black laminae (in hand sample) are composed of translucent silica in thin-section, constituting chalcedony and microcrystalline quartz in a mosaic arrangement. Moreover, the white to yellowish laminae (in hand sample) are isotropic and dark in thin-section, are more irregularly layered, and constitute kaolin clays that have replaced and cross-cut the silica layers (Fig. 7c). The F4.1 deposits also contain hollows (empty spaces, Fig. 7d), similar to those described for the F1 to F3 facies. Furthermore, the deposits preserve silica-cemented cracks in the white (in hand sample) kaolin clay material (Fig. 7d).

F4.2: shrubby lamination. This type of lamination was recognized where the original, shrubby or bushy stromatolitic fabrics were preserved. There are examples of excellent preservation (Fig. 7e, f), typically with variable amounts of patchy silica replacement. In contrast, there are areas of the F4.2 facies where it is difficult to distinguish the stromatolites because of strong silica replacement and holes (Fig. 7g). These latter examples also grade into the porous layered facies (F3). In hand sample, four different types of patchy diagenesis occur in these shrubby lamination (F4.2) samples, as evidenced by their colours and variable composition. First, the light-coloured (white to yellow in hand sample) shrubs are the reverse in colour, i.e. dark under plane-polarized light microscopy, and are composed of carbonate (right shrub of Fig. 7h). Second, reddish shrubs (in hand sample) are nearly opaque under the microscope, and contain a mixture of carbonate and iron oxides (Fig. 7i).

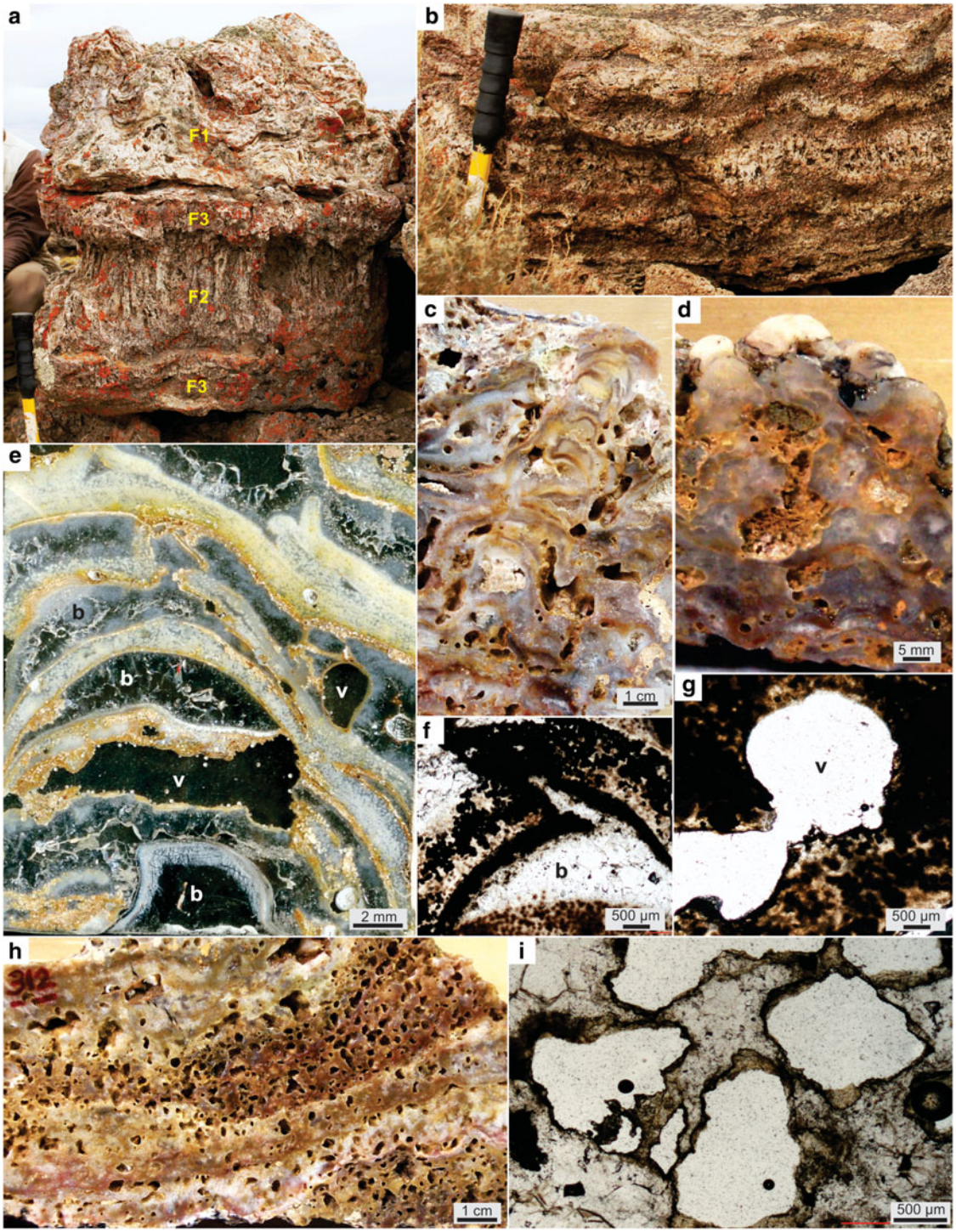

Figure 6. (Colour online) Photographs and photomicrographs of intercalated F2 and F3, vertical columnar structures and porous layers, respectively, at the Macanudo Norte Outcrop. All vertical section views. (a) Detail of the largest vertical columnar structures (F2) found in outcrop, in relation to interbedded F1 and F3 horizons. (b) Outcrop view (vertical section) of F2 and F3 intercalations. (c) Detail of the vertical columnar structures (F2). (d) Detail of the botryoidal variant of the vertical structures (F2). (e) Thin-section of the vertical columnar structures showing two types of voids: (1) inferred bubbles with almond shapes (b, partially or completely filled by translucent quartz) trapped within the growing stromatolite laminae, likely from microbial photosynthetic (oxygen) degassing (type 1, syn-depositional, concordant with laminae); and (2) etched voids (v, black, empty void space with irregular boundaries), formed by inferred acidic condensate corrosion and dissolution (type 2, post-depositional, discordant with laminae). (f) Void type 1 (b, inferred bubble), an amygdaloidal (almond-shaped) hollow filled with quartz, and broken at upper concave portion, likely due to fluid pressure. (g) Void type 2, an irregularly rounded hole (void space). (h) Hand sample of a porous layer (F3), with detail of lamination remnants. (i) Detail of dense, type 2 voids, typified by irregular margins and oxidation (red Fe-stained) rims, characterizing the porous layers (F3).

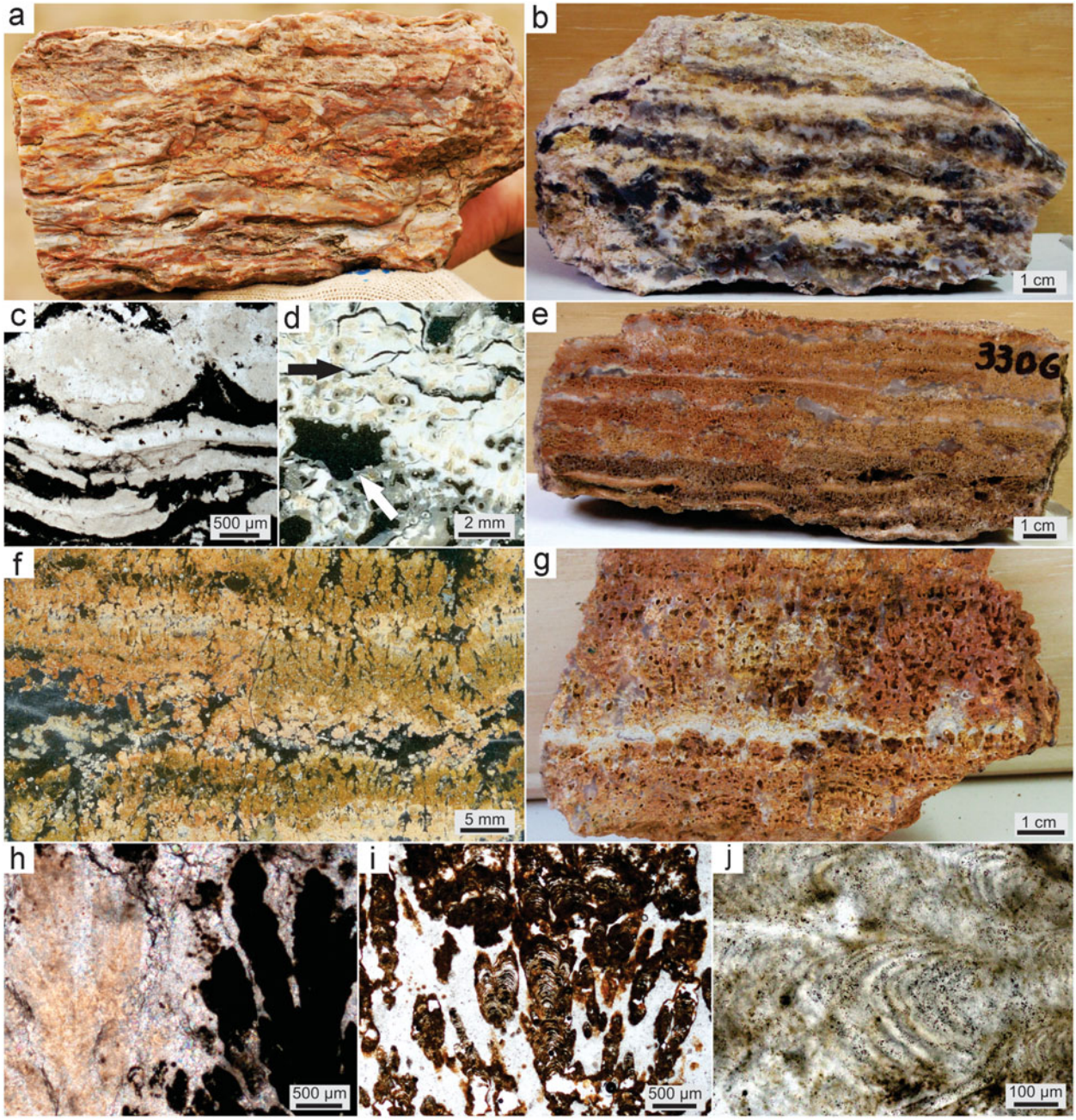

Figure 7. (Colour online) Photographs and photomicrographs of the lamination facies (F4) at Macanudo Norte Outcrop. All vertical section views. (a) Hand sample of travertine showing silica replacement, defined as pseudosinter by Guido & Campbell (2011). (b) Hand sample of irregular lamination (Facies 4.1), where white clay-rich and black silica-rich horizons can be distinguished; white horizons are inferred as products of late-stage hydrothermal alteration (e.g. acid–sulphate steam condensate infiltration). (c) Detail of F4.1, illustrating wavy laminated stromatolitic texture. (d) Detail of F4.1, illustrating the cracks sealed with silica in the clay-rich layers (black arrow) and a type 2 void (white arrow). (e, f) Hand sample slab and thin-section images of shrubby lamination (Facies 4.2), where thin (up to 0.5 cm high), 'bushy' dendritic stromatolites are evident. (g) Hand sample of an inferred acid-overprinted F4.2 example, showing strong development of secondary porosity (type 2 voids) (cf. Fig. 6). (h) Detail of shrubs of F4.2, some silicified (light coloured, left) and others (dark coloured, right) carbonate-rich with iron (cf. Fig. 11a–c). (i) Detail of the iron carbonate shrubs. (j) Detail of the silicified shrubs and their preserved internal texture.

Third, dark shrubs (black to brown in hand sample) are completely replaced by silica, and their translucent character under the microscope (left shrub of Fig. 7h) allows the stromatolitic textures to be seen in more detail at higher magnification (Fig. 7j). Fourth, some white areas within the dark shrubs (in hand sample) were observed to contain abundant chalcedony spheres under the microscope.

4.b.4. Facies 5 (F5): low-amplitude wavy bedding

This facies is present only at the Macanudo Sur Outcrop, and is mainly located beneath the mounds and breccias of Facies 6 (Fig. 4d, e), described below. The F5 facies is characterized by mesoscale, wavy and low-amplitude bedding that comprises parallel, ~1 cm thick lamination at the hand sample scale. These

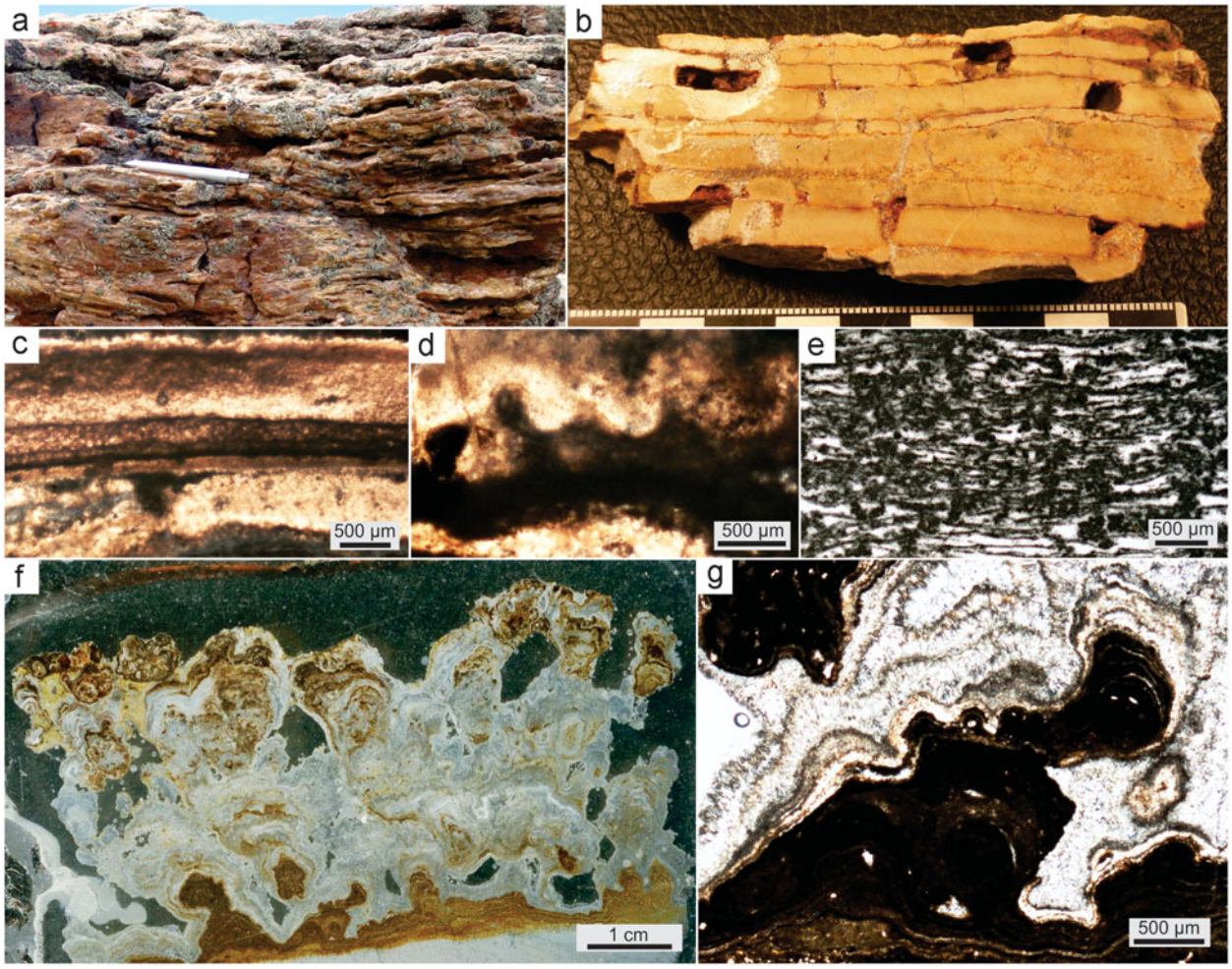

Figure 8. (Colour online) Photographs and photomicrographs of the low-amplitude wavy bedding (F5) at the Macanudo Sur Outcrop. All vertical section views; samples are dominantly composed of carbonate except for the silicified carbonate of (a). (a) Silicified upper portion of an outcrop, displaying pseudosinter texture; lenticular to blocky cavities (black) are surface-only features (i.e. weathering). (b) Hand sample slab showing thick laminae and thin beds forming wavy laminated carbonate. No primary or secondary porosity is evident (such as the two void types illustrated in Fig. 6), but rather the cavities in this sample (black empty spaces) formed from physical breakage associated with weathering of the outcrop. (c) Detail of the thick wavy lamination under the microscope. (d) Poorly preserved remnants of stromatolitic texture (dark, digitate morphology in micrite) in the wavy laminated facies. (e) Well-preserved, clotted and slightly wavy laminated, micritic fabric in F5, inferred as a microbial laminite. (f) Thin-section of a well-preserved, calcareous stromatolite horizon in F5. (g) Portion of the branching stromatolite in (f), comprising laminated micrite (dark reddish brown) with minor Fe, Mn, Mg, K and Si (Fig. 10d), encased in translucent bladed aragonite. Pen for scale is 13 cm long.

deposits are calcareous to siliceous in composition, and where silicified are another example of pseudosinter (Fig. 8a, b). Under the microscope, the parallel lamination is preserved as a generally massive texture (Fig. 8c), and contains uncommon, micritic, digitate, microstromatolitic growth morphologies (cumulate stratiform to knobby in outer form, Fig. 8d), as well as stylolite-like dissolution features, calcite veins and a rare, clotted-laminate micritic fabric (Fig. 8e). One of the samples shows well-preserved calcareous stromatolites (Fig. 8f), with an outer rim of tabular crystals of aragonite (Fig. 8g). This 1 cm thick stromatolitic horizon first grew from the substrate as cumulate to turbinate in form, transitioning upwards into columns displaying a lateral to dendroid branching style, and finally coalescing upwards to anastomosed branches with steeply convex to parabolic laminae.

4.b.5. Facies 6 (F6): mound and breccia features

This calcareous facies is only present in the Macanudo Sur area, positioned southwestwards along the length of the NNE-trending fault that links both outcrops. It is composed of mound-shaped bodies (Fig. 4d) with stromatolitic internal structures (Fig. 9a) and breccias (Fig. 9b).

4.c. EDS analyses

In order to confirm the chemical composition of the travertines, 19 EDS determinations were made on the different siliceous and calcareous facies described above. The analyses revealed a mixture of carbonates and silica in F1–F3 (e.g. Fig. 10a–c). Furthermore, silica replacement is prevalent in F4–F5, where we

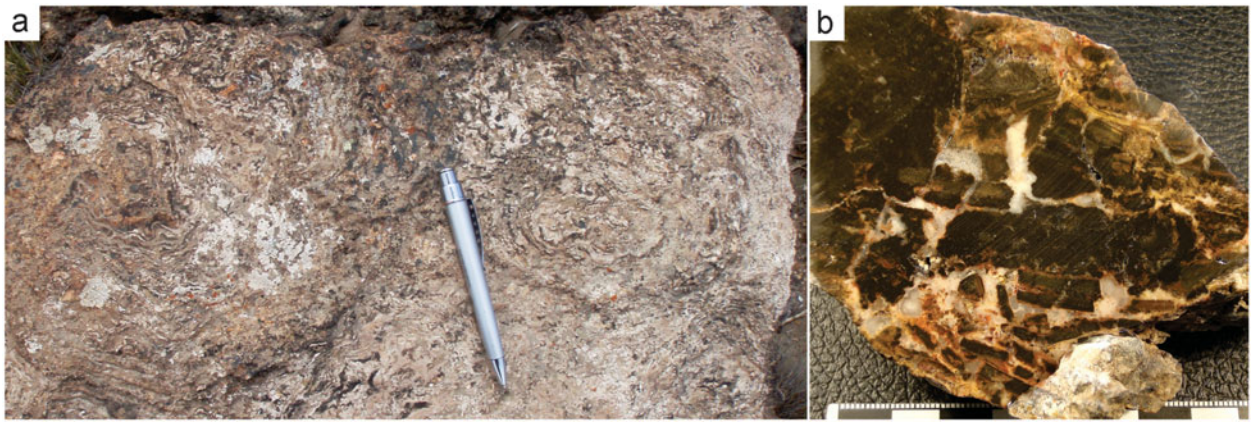

Figure 9. (Colour online) Photographs of the mound and breccia facies (F6) at the Macanudo Sur Outcrop. (a) Detail of the stromatolitic textures on top of a carbonate mound. (b) Hand sample slab of a hydrothermal breccia, with silicified travertine fragments (dark) and a quartz matrix (light). Pen for scale is 13 cm long.

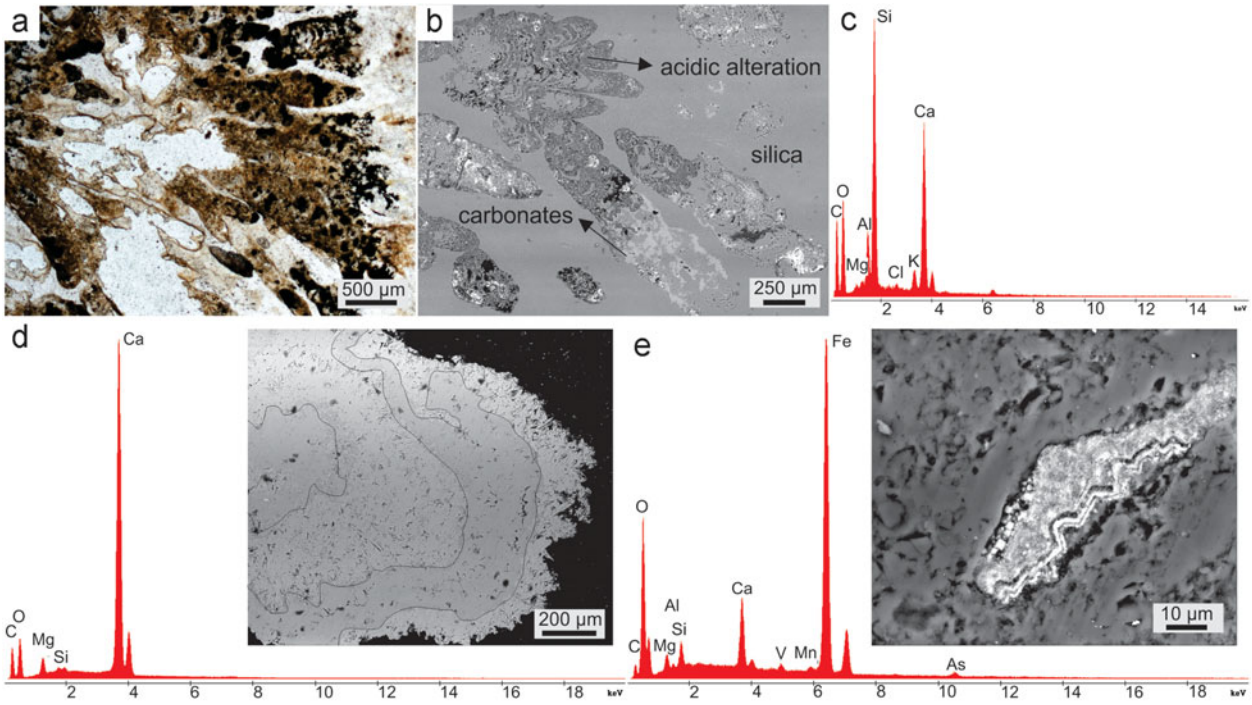

Figure 10. (Colour online) Photomicrographs, scanning electron microscope (SEM) backscatter images and EDS analyses from selected El Macanudo hot spring samples. (a, b) Shrubby lamination (F4.2), illustrating typical spatial relationship amongst carbonate (reddish brown), silicified (beige to translucent) and acid-altered (white, actual holes) portions of the sample. (c) EDS spectrum showing mixture of carbonate and silica. (d) EDS spectrum and SEM backscatter image of a stromatolitic carbonate-rich horizon (Fig. 8f, g), with Ca- and Mg-rich laminae (outlined with fine black lines). (e) EDS analysis and SEM backscatter image of a vug filled with siderite.

observed the texturally controlled transition between the two compositions. For F5 and F6, layers of Ca-rich and Mg-rich carbonates were detected (Fig. 10d), as well as siderite inclusions (Fig. 10e) in some portions of samples.

5. Discussion

5.a. Facies interpretation and modern analogues

By comparison with modern analogues and other fossil examples, the El Macanudo deposit may be inferred as a high-enthalpy, bicarbonate hot spring setting with subaqueous and subaerial components, and which contains a special travertine facies unique to the 23 Jurassic geothermal sites known from the Deseado Massif (Guido & Campbell, 2011): the large conical stromatolites (in the order of ~100 concentric cones in a 25 × 110 m area). In particular, these laminated, cone-shaped F1 structures (Figs 4b, 5) are interpreted as subaqueous spring-vents, with stromatolite growth features of up to 1 m in height that were forming in ~1–5 m deep pools, based on comparisons with domal columnar stromatolites growing within the Map of Africa hot pool (~50 °C) at Orakei Korako, New Zealand (cf. Drake *et al.* 2014, their fig. 9A, p. 30).

While this particular New Zealand example is from a sinter-forming geothermal setting, young (modern to sub-Recent) travertine analogues also occur at Yellowstone National Park (YNP) in the Mammoth Hot Springs area, and at sub-lacustrine springs in Nevada. Near Angel Terrace at YNP, we observed a small concentric cone structure (Fig. 11a) that was situated on the bottom of a small pool (now dry). Furthermore, groundwater spring-fed tufa in Big Soda Lake (Nevada, USA) also forms subaqueous, cone-shaped mounds (Rosen, Arehart & Lico, 2004, their fig. 3B, p. 410) similar to F1 at El Macanudo, which accumulate at a rapid rate ($\geq$ 30 mm yr^{-1}). The F1 travertine conduits are preserved in silica, and are riddled with holes (Fig. 5c–e) that overprint the original crenulated to wavy, laminated, concentric stromatolitic fabric. The holes may represent dissolution produced by escaping acidic gases, discussed further below.

The F2 and F3 facies (Figs 4b, 6) are also inferred as subaqueous stromatolitic features, having developed their variable layering during growth in pools, in shallower water than F1, such that the thickness of each F2 and F3 layer appears to reflect the depth of water at the time of their formation. Figure 11b illustrates vertical columnar structures similar to F2 and F3 (cf. Fig. 6b) from an extinct, eroded, sub-Recent terrace margin near Angel Terrace at YNP. Figures 4b and 6a show a portion of the stratigraphy from Macanudo Norte, illustrating a deepening from the shallow pool setting of F2 and F3 at the base, developing upwards into the F1 spring-pool stromatolitic cones. Like F1, the F2 and F3 facies also display a strong silica overprint (Fig. 6c–e). The features preserve two types of holes (Fig. 6e–i), indicating two different kinds of gas-related events. The first is construed to have trapped gases during hot spring formation, which occasionally broke partition walls (Fig. 6f; type 1 concordant with laminations, mainly within F2). They may have been formed by photosynthetic gas release as they are enclosed within the inferred columnar stromatolitic textures and are similar to 'bubble mats' of mid-apron (travertine, sinter) settings (e.g. Hinman & Lindstrom, 1996; Campbell *et al.* 2001; Guido & Campbell, 2009; Guido *et al.* 2010; Guido & Campbell, 2011, 2012). The second type of hole is surmised to have been caused by late diagenetic dissolution owing to etching by acidic gases (Fig. 6g–i; type 2 discordant with lamination, and affecting both F2 and F3).

The F4 irregular and shrubby lamination features (Figs 4c, 7) are interpreted as subaerial travertine terraces in a mid- to distal apron setting. On the modern travertine apron at Minerva Terrace (YNP), parallel laminae and beds are common (Fig. 11c), with well-preserved, microbe-coated, shrubby stromatolitic textures evident in shallow terrace pools atop Minerva Terrace (Fig. 11d), and in nearby dried pools of sub-Recent samples (Fig. 11e). Travertine shrubs, or bushes, are well known from shallow terracette pools of modern and Cenozoic hot spring settings, including YNP, German, Italian and other sites (e.g. Chafetz & Folk, 1984; Pentecost, 1990; Koban & Schweigert, 1993; Guo & Riding, 1994; Chafetz & Guidry, 1999; Fouke *et al*. 2000). Over more than a century of observation, these shrubby travertine fabrics have been variably interpreted as abiogenic or bacterial in origin (Pentecost, 1990). The small volumes of organic matter extracted from modern travertine (Pentecost, 1990) and the occlusion of microbial filaments or moulds by abiotic mineralization or post-depositional recrystallization (Chafetz & Guidry, 1999) have led some to conclude that the shrubs develop by inorganic processes. However, detailed textural study of a wide variety (age, location, mineralogy) of samples by Chafetz & Guidry (1999) concluded that microbes act as catalysts for mineralization of all shrubby travertine fabrics, grading from strongly arborescent shrubs (bacterial influence dominates morphology) to geometric crystal shrubs (crystalline habit governed by physicochemical processes, but with bacterial clumps or their moulds at their centres). At El Macanudo, only those F4 travertine-terrace fabrics that underwent early silicification (e.g. Fig. 7i, j; represented by dark shrubs in hand sample that are translucent under the microscope) have preserved some of the details of the original, laminated, arborescent bacterial stromatolites. Otherwise, acidic pore fluids preferentially affected the shrubby portions of the laminations (Figs. 7g–i), recrystallizing the carbonate and creating the etched cavities as described for F1–F3, in some cases causing fabric-selective dissolution of shrub interiors while maintaining their broad outlines. The late acidic hydrothermal fluids also were injected into the irregular laminated facies (F4.2) and deposited kaolin clays (white in hand sample and dark in thin-section; e.g. Fig. 7a–d) parallel to and crossing bedding.

Facies 5 and 6 are spatially associated with each other in the Macanudo Sur area, and are interpreted as wavy bedded, subaerial travertine slope deposits (F5) overlain by travertine mound (F6) deposits (e.g. Fig. 4d, e). In the Angel Terrace area of YNP, we found sub-Recent vent mounds (Fig. 11f) with stromatolitic growth on top and low-amplitude wavy bedding adjacent to and beneath the mound features (e.g. Fig. 11g). The F6 Macanudo mounds comprise crenulated, concentric stromatolitic features on top (Fig. 9a) and localized breccia in the core of the vent, visible where the mounds are eroded (Fig. 9b). This F6 facies can be compared with F1 in that both indicate proximity to vent areas and had stromatolites growing around the vents, but one developed cones under water (F1) and the other formed mounds on land (F6).

The inferred features of steam-heated acidic overprinting of the El Macanudo hot spring deposits, as deduced from the ubiquitous hollows and irregularly porous textures that riddle F1–F4, in particular, have analogues in the geothermal fields of the Taupo Volcanic Zone, New Zealand. Tikitere (Hell's Gate), Te Kopia and Ngapouri contain comparable examples, where acidic steam condensate overprints siliceous

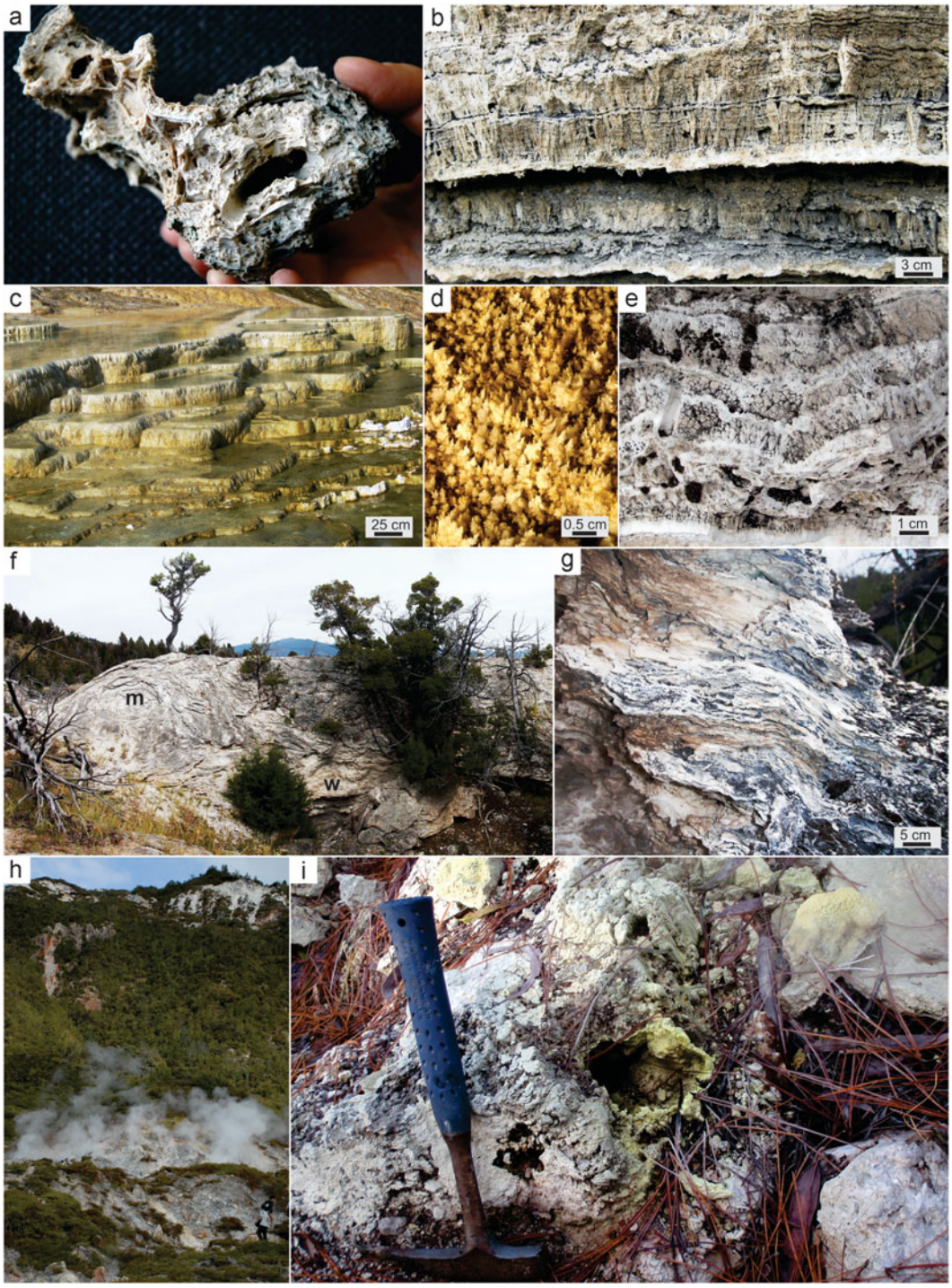

Figure 11. (Colour online) Photographs of modern to sub-Recent analogues for the Jurassic El Macanudo travertine deposit. (a–f) are from Mammoth Hot Springs, Yellowstone National Park, USA, and (g) and (h) are from the Taupo Volcanic Zone (TVZ), New Zealand. (a) Two small-scale, laterally concentric cones (viewed from their bases) from the Angel Terrace area, found in a recently dried, small pool (~2 m diameter). Compare to Figure 5a, inset. (b) Regular lamination in thinly bedded, vertical columnar structures, and intercalated with massive banded horizons, from the Angel Terrace area. Compare to Figures 4b and 6b. (c) Typical small travertine terraces forming on Minerva Terrace, which are internally laminated. (d) Modern shrub photo in a few centimetres of spring water, from the top of one modern terrace pool. (e) Detail of recently fossilized shrubby lamination from the Angel Terrace area. Compare to Figure 7e, f. (f) Calcareous mound (m) and adjacent, low-amplitude wavy bedding (w), from the Angel Terrace area. Compare to the Macanudo Sur Outcrop facies distributions map (Fig. 3) and Figure 4d, e. (g) Detail of low-amplitude wavy bedding at the base of a mound, from the Angel Terrace area. Compare to Figure 4d. (h) Overview of acid steam-heated altered sinter (steaming fumaroles around landslide blocks) and hydrothermally altered volcanic rocks (red and white patches in upper vegetated area) in cliffs along the active Paeroa Fault at Te Kopia, TVZ. (i) Detail of yellow, sulphur-lined fumarolic conduits and hollows (dark holes) developed in modern to sub-Recent sinter due to acid overprinting (Ngapouri sinter, TVZ). Hammer for scale is 40 cm long.

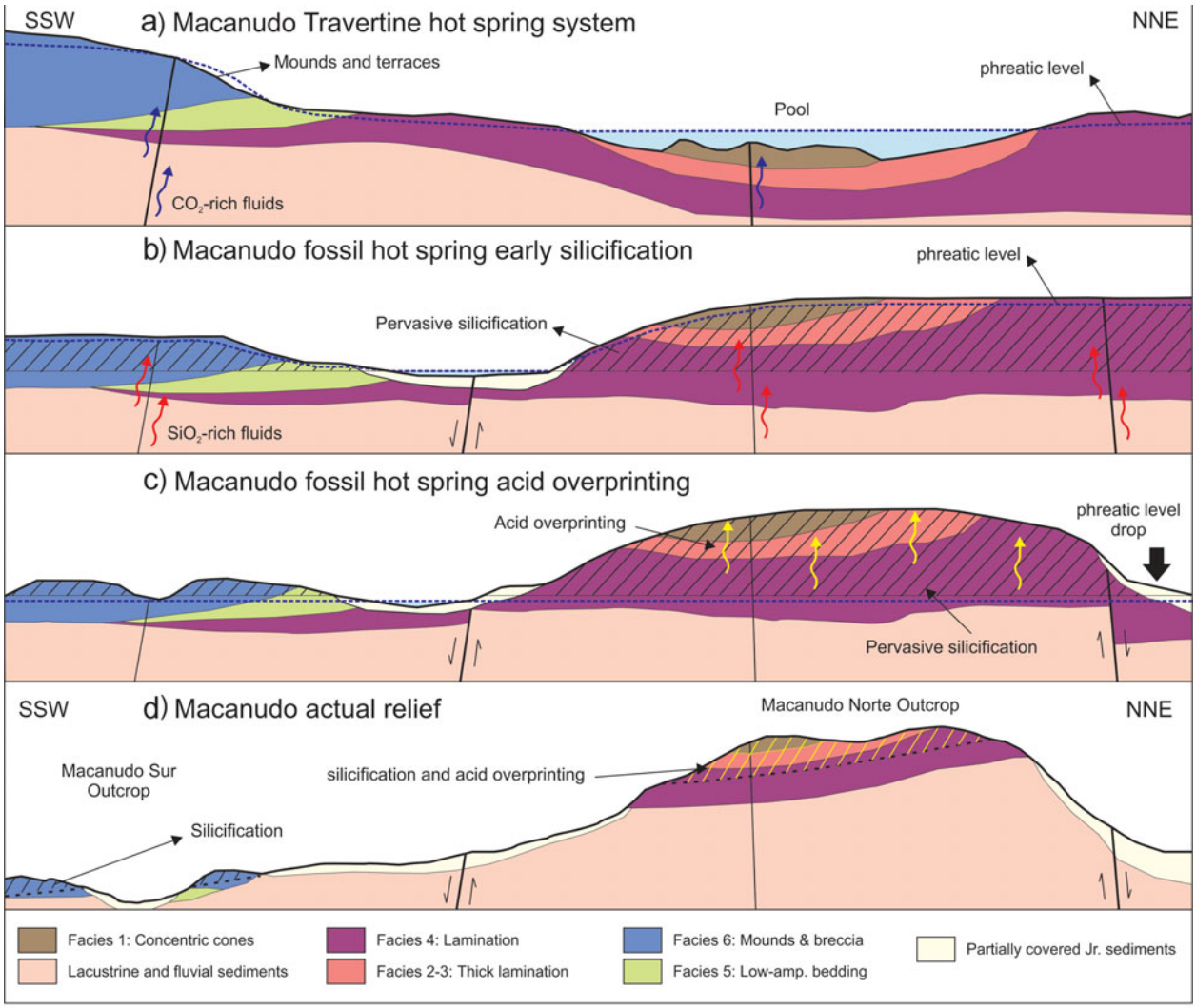

Figure 12. (Colour online) (a–d) Schematic NNE–SSW cross-section along Macanudo Norte and Macanudo Sur outcrops and their evolution from Late Jurassic to Recent times to produce the inverted topography and mineralization pattern seen today. Details in text.

hot spring deposits and adjacent rocks (Fig. 11h), creating gas escape hollows and precipitating native sulphur (Fig 11i).

5.b. Evolutionary history of the Jurassic El Macanudo geothermal system

El Macanudo provides an opportunity to assess the impact of depositional and post-depositional history on fossil (150 Ma) hot spring microfacies and on the microbial fossil preservation state of thermogene travertines in the geological record. A detailed evolutionary history may be constructed (Fig. 12) because of the structurally undisturbed nature of the Jurassic deposit. Their detailed mapping and paragenetic study, described herein, indicate spatial and topographic relationships amongst travertine formation, its early silicification and the late-stage acid overprinting features and their distributions.

The Mirasol low area at El Macanudo (Fig. 2) is interpreted as having been a high-relief area during Cenozoic times, since it was not covered by the surrounding Eocene flood basalts. This high-relief area could have been a Jurassic volcanic centre that was subsequently intensely eroded because the younger basalts flowed outwards from faults along the NE, NW and SE borders of the Mirasol low area (Fig. 2). Such erosion could have been enhanced in areas of Late Jurassic hydrothermal alteration, which may have physically and chemically weakened the rocks within the pseudosinters (silicified travertines) and travertines of the Macanudo palaeo-hot spring area. The southern ignimbrite (Fig. 2) also flowed along a NE–SW-oriented, high-palaeo-relief area that was not covered by basalts. It probably travelled towards the SW, away from the interpreted volcanic centre in the Mirasol low area, and exhibits a Jurassic SW-dipping slope. This general geological affiliation of aligned ignimbrites and hot springs is also regionally consistent with the Flecha Negra ignimbrite flow in the La Esperanza area (Echeveste *et al.* 1999, FN of Fig. 1), about 50 km south of Macanudo, which is close to the Jurassic Cerro Tornillo hot spring area (Mykietiuk & Lanfrancini, 2004, CT of Fig. 1).

As discussed in Section 5.a, the El Macanudo petrographic and mineralogical observations of this study (Figs 5–10) confirm that the siliceous facies are carbonates replaced by silica, as was proposed by Schalamuk *et al*. (1999). Specifically, Facies 1–4, the subaqueous travertine pool and surrounding subaerial travertine apron terrace associations of Macanudo Norte are composed of silica with few calcareous relics. In addition, the subaerial travertine mound facies associations of Macanudo Sur (F5, F6) are mainly calcareous, showing only patchy silicification of these mound deposit affiliations, with remnant microbial stromatolite and laminate fabrics (Fig. 8d, e) in the F5 wavy bedding found at the base of subaerial mounds. Some relict stromatolite morphologies (branched columnar) also are preserved in carbonate where there is partial iron replacement and coating by a fibrous cement (Fig. 8f, g), but even so their internal fine laminae have been recrystallized. Some travertine bacterial shrubs from elsewhere also have been moderately well preserved by similar sparry cement coatings (cf. Chafetz & Guidry, 1999, their fig. 5d, p. 64).

Considering the El Macanudo travertine facies and their mineralogical distributions with respect to topography, a silica cap replacement likely developed in the area at approximately the 660 m topographic limit (Fig. 3). Detailed mapping, together with strike and dip measurements of primary sedimentary layering, shows structurally controlled vent areas at both northern and southern outcrops, mainly located along regional NNE- and ENE-trending faults, with another interpreted vent source north of the Macanudo Norte Outcrop, but not preserved (Fig. 3). Strike and dip measurements from *in situ* outcrops of the hot spring deposits (e.g. Fig. 4c) indicate a concentric distribution of travertine facies with respect to the two interpreted vent areas: ENE-oriented F1 at the Macanudo Norte Outcrop, and NNE-oriented F6 at the Macanudo Sur Outcrop. The Macanudo Norte Outcrop rocks represent a silica-replaced travertine apron sequence at a higher palaeo-elevation (preserved also in the present day; Fig. 3), with development of large subaqueous stromatolites in a deep travertine-terrace pool or in a shallow, geothermally influenced lacustrine environment; whereas, the Macanudo Sur Outcrop represents a subaerial travertine mound sequence. The lower topographic limit of pervasive regional silicification was also mapped for both outcrops (Fig. 3). Early silicification was responsible for exceptional preservation of some fabrics and stromatolitic structures, especially in the Macanudo Norte Outcrop area, but most were largely affected by a later steam-heated system, probably due to a drop of the palaeo-phreatic surface, which subsequently produced the intense argillization of the host rocks and the acid dissolution hollows observed in Macanudo Norte F1–F4 travertine.

Figure 12 illustrates our interpretation of the evolutionary history of the El Macanudo silica-carbonate deposit. Three different events occurred during Late Jurassic time at El Macanudo (Fig. 12a–c) that were related to the large and long-lasting hydrothermal systems active across the Deseado Massif at this time. Themogene travertines were primarily precipitating in a conventional hot-spring-related geothermal system (see fig. 3B in Guido & Campbell, 2011), with subaerial mound products in the south, and subaqueous pool and surrounding subaerial terrace features forming in the north (Fig. 12a). Subsequently, active faulting impacted on the CO_2-rich geothermal system, introducing pervasive silicification that was probably related to regional migration of silica-saturated hydrothermal fluids (Fig. 12b). This was the time when exceptional preservation of some shrubby bacterial stromatolites likely occurred. Following this extensive silicification episode, a change in palaeo-phreatic water level commenced. A drop in the water table exposed the northern part of the outcrops to acid alteration (Fig. 12c). Then, this area was probably partially covered by friable Cretaceous and Tertiary sedimentary deposits that were eroded by regional uplift of the entire massif (Guido & Campbell, 2011), exposing today these slightly tilted Jurassic palaeo-surfaces (Fig. 12d).

5.c. Implications for the preservation of Lagerstätte in the extreme (palaeo)environments of fossil hot springs

Because fossil microbial preservation is less likely in thermogene travertines compared to siliceous sinters, owing to ready neomorphism and other diagenetic effects in carbonates, sinters are more likely to produce fossil Lagerstätte, such as in the Jurassic San Agustín sinter in the Deseado Massif (SA of Fig. 1) (Guido *et al.* 2010; Channing *et al*. 2011; García Massini *et al.* 2012) and the Devonian Rhynie Chert in Scotland (Trewin, 1996 and references therein). Silicification of some thermogene travertines of the Deseado Massif has preserved microbial structures well at the micro-scale, as in the Cerro Negro deposit (CN of Fig. 1; Guido & Campbell, 2012), and the silicified bacterial shrubs described here from El Macanudo. However, for such high-quality preservation to occur, these pseudosinters had to have silicified early during diagenesis; otherwise, carbonate weathering, hydrothermal alteration and/or burial diagenesis would have eliminated fine-scale microbial and other primary features before they could be preserved by subsequent silicification or other mineralization. Finally, we note that those silicified travertines and sinters in the Deseado Massif that are free from late-stage acid alteration signatures also tend to have moderate to excellent lithofacies and biofacies preservation (e.g. La Marciana, San Agustín, Claudia, Cerro Negro; Fig. 1; Guido & Campbell, 2011), and thus we predict a similar pattern may hold for other palaeo-geothermal deposits elsewhere in the world.

Acknowledgements. We thank INREMI and The University of Auckland for institutional and other support. Funding was provided by the National Geographic Society, Subsidios

Automáticos and PICT. Alan Channing, Jack Farmer, Nancy Hinman and Pat Browne furnished field logistical assistance and fruitful discussions. We are grateful to two anonymous reviewers who improved the quality of the manuscript.

References

Cady, S. L. & Farmer, J. D. 1996. Fossilization processes in siliceous thermal springs: trends in preservation along thermal gradients. In *Evolution of Hydrothermal Ecosystems on Earth (and Mars?)* (eds G. R. Bock & G. A. Goode), pp. 150–73. Proceedings of the Ciba Foundation Symposium 202. Chichester: J. Wiley.

Campbell, K. A., Guido, D. M., Gautret, P., Foucher, F., Ramboz, C. & Westall, F. 2015a. Geyserite in hot-spring siliceous sinter: window on Earth's hottest terrestrial paleoenvironment and its extreme life. *Earth-Science Reviews* **148**, 44–64.

Campbell, K. A., Lynne, B. Y., Handley, K., Jordan, S., Farmer, J., Guido, D., Turner, S. & Perry, R. 2015b. Tracing biosignature preservation of geothermally silicified microbial textures into the geological record. *Astrobiology* **15**, 858–82.

Campbell, K. A., Sannazzaro, K., Rodgers, K. A., Herdianita, N. R. & Browne, P. R. L. 2001. Sedimentary facies and mineralogy of the late Pleistocene Umukuri silica sinter, Taupo Volcanic Zone, New Zealand. *Journal of Sedimentary Research* **71**, 727–46.

Chafetz, H. S. & Folk, R. L. 1984. Travertines: depositional morphology and the bacterially constructed constituents. *Journal of Sedimentary Petrography* **54**, 289–316.

Chafetz, H. S. & Guidry, S. A. 1999. Bacterial shrubs, crystal shrubs, and ray-crystal shrubs: bacterial vs. abiotic precipitation. *Sedimentary Geology* **126**, 57–74.

Channing, A., Zamuner, A., Edwards, D. & Guido, D. 2011. *Equisetum thermale* sp. nov. (Equisetales) from the Jurassic San Agustín hot spring deposit, Patagonia: anatomy, paleoecology and inferred paleoecophysiology. *American Journal of Botany* **98**, 680–97.

Drake, B. D., Campbell, K. A., Rowland, J. V., Guido, D. M., Browne, P. R. L. & Rae, A. 2014. Evolution of a dynamic paleo-hydrothermal system at Mangatete, Taupo Volcanic Zone, New Zealand. *Journal of Volcanology and Geothermal Research* **282**, 19–35.

Echeveste, H., Fernández, R., Bellieni, G., Tessone, M., Llambias, E., Schalamuk, I., Piccirillo, E. & De Min, A. 2001. Relaciones entre las Formaciones Bajo Pobre y Chon Aike (Jurásico medio a superior) en el área de Estancia El Fénix-Cerro Huemul, zona centro-occidental del Macizo del Deseado, provincia de Santa Cruz. *Revista de la Asociación Geológica Argentina* **56**(4), 548–58.

Echeveste, H., Fernández, R., Llambias, E., Tessone, M., Schalamuk, I., Bellieni, G., Piccirillo, E. & De Min, A. 1999. Ignimbritas tardías de alto grado en la Formación Chon Aike (Jurásico). Macizo del Deseado, Santa Cruz. Argentina. In *XIV Congreso Geológico Argentino, Actas II*, pp. 182–5.

Ellis, A. J. & Wilson, S. H. 1961. Hot spring areas with acid–sulphate–chloride waters. *Nature* **191**, 696–8.

Farmer, J. D. 2000. Hydrothermal systems: doorways to early biosphere evolution. *GSA Today* **10**, 1–9.

Feruglio, E. 1949. *Descripción Geológica de la Patagonia*. Dirección Nacional de Yacimientos Petrolíferos Fiscales, Buenos Aires, Tomo 1, pp. 17–19.

Fouke, B. W., Farmer, J. D., Des Marais, D. J., Pratt, L., Sturchio, N. C., Burns, P. C. & Discipulo, M. K. 2000. Depositional facies and aqueous-solid geochemistry of travertine depositing hot springs (Angel Terrace, Mammoth Hot Springs, Yellowstone National Park, U.S.A.). *Journal of Sedimentary Research* **70**, 565–85.

Fournier, R. O. 1985. The behaviour of silica in hydrothermal solutions. *Reviews in Economic Geology* **2**, 45–62.

Fournier, R. O. & Rowe, J. J. 1966. Estimation of underground temperatures from the silica content of water from hot springs and steam wells. *American Journal of Science* **264**, 685–97.

García Massini, J., Channing, A., Guido, D. M. & Zamuner, A. B. 2012. First report of fungi and fungus-like organisms from Mesozoic hot springs. *Palaios* **27**, 55–62.

Giacosa, R., Zubia, M., Sánchez, M. & Allard, J. 2010. Meso-Cenozoic tectonics of the southern Patagonian foreland: structural evolution and implications for Au-Ag veins in the eastern Deseado region (Santa Cruz, Argentina). *Journal of South American Earth Sciences* **30**, 134–50.

Gibert, R. O., Taberner, C., Sáez, A., Giralt, S., Alonso, R. N., Edwards, R. L. & Pueyo, J. J. 2009. Igneous origin of CO_2 in ancient and recent hot-spring waters and travertines from the northern Argentinean Andes. *Journal of Sedimentary Research* **79**, 554–67.

Guido, D. 2004. Subdivisión litofacial e interpretación del volcanismo jurásico (Grupo Bahía Laura) en el este del Macizo del Deseado, provincia de Santa Cruz. *Revista de la Asociación Geológica Argentina* **59**(4), 727–42.

Guido, D. M. & Campbell, K. A. 2009. Jurassic hot-spring activity in a fluvial setting at La Marciana, Patagonia, Argentina. *Geological Magazine* **146**, 617–22.

Guido, D. M. & Campbell, K. A. 2011. Jurassic hot spring deposits of the Deseado Massif (Patagonia, Argentina): characteristics and controls on regional distribution. *Journal of Volcanology and Geothermal Research* **203**, 35–47.

Guido, D. M. & Campbell, K. A. 2012. Diverse subaerial and sublacustrine hot springs setting of the Cerro Negro epithermal (Jurassic, Deseado Massif), Patagonia, Argentina. *Journal of Volcanology and Geothermal Research* **229–230**, 1–12.

Guido, D. M. & Campbell, K. A. 2014. A large and complete Jurassic geothermal field at Claudia, Deseado Massif, Santa Cruz, Argentina. *Journal of Volcanology and Geothermal Research* **275**, 61–70.

Guido, D. M., Channing, A., Campbell, K. A. & Zamuner, A. 2010. Jurassic geothermal landscapes and fossil ecosystems at San Agustín, Patagonia, Argentina. *Journal of the Geological Society, London* **167**, 11–20.

Guido, D., Delupí, R., López, R., de Barrio, R. & Schalamuk, I. 2002. Estromatolitos y mineralización epitermal en el área Marianas-Eureka, Macizo del Deseado, Santa Cruz. In *XV Congreso Geológico Argentino, Calafate, Actas II*, pp. 284–9.

Guido, D., Escayola, M., de Barrio, R., Schalamuk, I. & Franz, G. 2006. La Formación Bajo Pobre (Jurásico) en el este del Macizo del Deseado, Patagonia: vinculación con el Grupo Bahía Laura. *Revista de la Asociación Geológica Argentina* **61**(2), 187–96.

Guido, D. & Schalamuk, I. 2003. Genesis and exploration potential of epithermal deposits from the Deseado Massif, Argentinean Patagonia. In *Mineral Exploration and*

Sustainable Development (eds D. Eliopoulos *et al.*), pp. 489–92. Rotterdam: Millpress.

Guo, L. & Riding, R. 1994. Origin and diagenesis of Quaternary travertine shrub fabrics, Rapolano Terme, central Italy. *Sedimentology* **41**, 499–520.

Handley, K. & Campbell, K. A. 2011. Character, analysis and preservation of biogenicity in terrestrial siliceous stromatolites from geothermal settings. In *Stromatolites: Interaction of Microbes with Sediments* (eds V. Tewari & J. Seckbach), pp. 359–81. Cellular Origin, Life in Extreme Habitats and Astrobiology 18. Dordrecht: Springer.

Henley, R. W. & Ellis, A. J. 1983. Geothermal systems, ancient and modern: a geochemical review. *Earth-Science Reviews* **19**, 1–50.

Herdianita, N. R., Browne, P. R. L., Rodgers, K. A. & Campbell, K. A. 2000. Mineralogical and textural changes accompanying ageing of silica sinter. *Mineralium Deposita* **35**, 48–62.

Hinman, N. W. & Lindstrom, R. F. 1996. Seasonal changes in silica deposition in hot spring systems. *Chemical Geology* **132**, 237–46.

Jones, B. & Renaut, R. W. 2003a. Petrography and genesis of spicular and columnar geyserite from the Whakarewarewa and Orakeikorako geothermal areas, North Island, New Zealand. *Canadian Journal of Earth Science* **40**, 1585–610.

Jones, B. & Renaut, R. W. 2003b. Hot spring and geyser sinters: the integrated product of precipitation, replacement, and deposition. *Canadian Journal of Earth Science* **40**, 1549–69.

Jones, B. & Renaut, R. W. 2010. Calcareous spring deposits in continental settings. In *Carbonates in Continental Settings: Facies, Environments & Processes* (eds A. M. Alonso-Zarza & L. H. Tanner), pp. 177–224. Developments in Sedimentology 61. Amsterdam: Elsevier.

Jones, B. & Renaut, R. W. 2011. Hot springs and geysers. In *Encyclopedia of Geobiology* (eds J. Reitner & V. Thiel), pp. 447–51. Heidelberg: Springer.

Jones, B. & Renaut, R. W. 2012. Facies architecture in depositional systems resulting from the interaction of acidic springs, alkaline springs, and acidic lakes: case study of Lake Roto-a-Tamaheke, Rotorua, New Zealand. *Canadian Journal of Earth Science* **49**, 1217–50.

Jones, B., Renaut, R. W. & Owen, B. O. 2011. Life of a geyser discharge apron: evidence from Waikite Geyser, Whakarewarewa geothermal area, North Island, New Zealand. *Sedimentary Geology* **236**, 77–94.

Koban, C. G. & Schweigert, G. 1993. Microbial origin of travertine fabrics – two examples from Southern Germany (Pleistocene Stuttgart travertines and Miocene Riedöschingen travertine). *Facies* **29**, 251–64.

Lynne, B. Y. 2012. Mapping vent to distal-apron hot spring paleo-flow pathways using siliceous sinter architecture. *Geothermics* **43**, 3–24.

Lynne, B. Y. & Campbell, K. A. 2003. Diagenetic transformations (opal-A to quartz) of low and mid-temperature microbial textures in siliceous hot-spring deposits, Taupo Volcanic Zone, New Zealand. *Canadian Journal of Earth Sciences* **40**, 1679–96.

Lynne, B. Y., Campbell, K. A., James, B. J., Browne, P. R. L. & Moore, J. 2007. Tracking crystallinity in siliceous hot-spring deposits. *American Journal of Science* **307**, 612–41.

Lynne, B. Y., Campbell, K. A., Moore, J. N. & Browne, P. R. L. 2005. Diagenesis of 1900-year-old siliceous sinter (opal-A to quartz) at Opal Mound, Roosevelt Hot Springs, Utah, U.S.A. *Sedimentary Geology* **179**, 249–78.

Lynne, B. Y., Campbell, K. A., Moore, J. & Browne, P. R. L. 2008. Origin and evolution of the Steamboat Springs siliceous sinter deposit, Nevada, U.S.A. *Sedimentary Geology* **210**, 111–31.

Lynne, B. Y., Campbell, K. A., Perry, R. S., Browne, P. R. L. & Moore, J. N. 2006. Acceleration of sinter diagenesis in an active fumarole, Taupo Volcanic Zone, New Zealand. *Geology* **34**, 749–52.

Mykietiuk, K. & Lanfrancini, M. 2004. Depósitos Jurásicos de un lago geotermal en el Cerro Tornillo, Macizo del Deseado, Santa Cruz. In *7 Congreso de Mineralogía y Metalogenia*, pp. 261–6.

Nicholson, K. 1993. *Geothermal Fluids: Chemistry and Exploration Technique*. Berlin: Springer.

Pankhurst, R. J., Leat, P. T., Sruoga, P., Rapela, C. W., Marquez, M., Storey, B. C. & Riley, T. R. 1998. The Chon Aike province of Patagonia and related rocks in West Antarctica: a silicic large igneous province. *Journal of Volcanology and Geothermal Research* **81**, 113–36.

Pentecost, A. 1990. The formation of travertine shrubs: Mammoth Hot Springs, Wyoming. *Geological Magazine* **127**, 159–68.

Pentecost, A. 1993. British travertines: a review. *Proceedings of the Geologists' Association* **104**, 29–39.

Pentecost, A. 2005. *Travertine*. Berlin: Springer, 445 pp.

Renaut, R. W. & Jones, B. 2000. Microbial precipitates around continental hot springs and geysers. In *Microbial Sediments* (eds R. Riding & S. M. Awramik), pp. 187–95. Berlin: Springer.

Renaut, R. W. & Jones, B. 2011a. Hydrothermal environments, terrestrial. In *Encyclopedia of Geobiology* (eds J. Reitner & V. Thiel), pp. 467–79. Heidelberg: Springer.

Renaut, R. W. & Jones, B. 2011b. Sinter. In *Encyclopedia of Geobiology* (eds J. Reitner & V. Thiel), pp. 808–13. Heidelberg: Springer.

Renaut, R. W., Morley, C. K. & Jones, B. 2002. Fossil hot-spring travertine in the Turkana basin, northern Kenya: Structure, facies, and genesis. In *Sedimentation in Continental Rifts* (eds R. W. Renaut & G. M. Ashley), pp. 123–41. SEPM Special Publication no. 73.

Richardson, N. J. & Underhill, J. R. 2002. Controls on the structural architecture and sedimentary character of syn-rift sequences, North Falkland Basin, South Atlantic. *Marine and Petroleum Geology* **19**, 417–43.

Rodgers, K. A., Browne, P. R. L., Buddle, T. F., Cook, K. L., Greatrex, R. A., Hampton, W. A., Herdianita, N. R., Holland, G. R., Lynne, B. Y., Martin, R., Newton, Z., Pastars, D., Sannazarro, K. L. & Teece, C. I. A. 2004. Silica phases in sinters and residues from geothermal fields of New Zealand. *Earth-Science Reviews* **66**, 1–61.

Rosen, M. R., Arehart, G. B. & Lico, M. S. 2004. Exceptionally fast growth rate of <100-year-old tufa, Big Soda Lake, Nevada: implications for using tufa as a paleoclimate proxy. *Geology* **32**, 409–12.

Rowland, J. V. & Simmons, S. F. 2012. Hydrologic, magmatic, and tectonic controls on hydrothermal flow, Taupo Volcanic Zone, New Zealand: implications for the formation of epithermal vein deposits. *Economic Geology* **107**(3), 427–57.

Schalamuk, I. B., Guido, D. M., de Barrio, R. E. & Fernandez, R. R. 1999. Hot spring structures from El

Macanudo-El Mirasol area, Deseado Massif, Argentina. In *Mineral Deposits: Processes to Processing* (eds C. J. Stanley, *et al*.), pp. 577–80. Rotterdam: Balkema.

Schalamuk, I. B., Zubia, M., Genini, A. & Fernández, R. R. 1997. Jurassic epithermal Au-Ag deposits of Patagonia, Argentina. *Ore Geology Reviews* **12**, 173–86.

Schinteie, R., Campbell, K. A. & Browne, P. R. L. 2007. Microfacies of stromatolitic sinter from acid–sulphate–chloride springs at Parariki Stream, Rotokawa geothermal field, New Zealand. *Palaeontologia Electronica* **10**(1), 1–33 (4A), http://palaeoelectronica.org/paleo/2007_1/sinter/index.html.

Sibson, R. H. 1987. Earthquake rupturing as a mineralizing agent in hydrothermal systems. *Geology* **15**, 701–4.

Sillitoe, R. H. 2015. Epithermal paleosurfaces. *Mineralium Deposita* **50**, 767–93.

Sturchio, N. C., Dunkley, P. N. & Smith, M. 1993. Climate-driven variations in the geothermal activity of the northern Kenya Rift Valley. *Nature* **362**, 233–4.

Trewin, N. H. 1996. The Rhynie Chert: an early Devonian ecosystem preserved by hydrothermal activity. In *Evolution of Hydrothermal Ecosystems on Earth (and Mars?)* (eds G. R. Bock & G. A. Goode), pp. 131–49. Proceedings of the Ciba Foundation Symposium 202. Chichester: J. Wiley.

Trewin, N. H., Fayers, S. R. & Kelman, R. 2003. Subaqueous silicification of the contents of small ponds in an early Devonian hot spring complex, Rhynie, Scotland. *Canadian Journal of Earth Science* **40**, 1697–712.

White, D. E. 1967. Some principles of geyser activity, mainly from Steamboat Springs, Nevada. *American Journal of Science* **265**, 641–84.